Universitas Carolina Pragensis

Facultas Mathematica Physicaque

Magister thesis

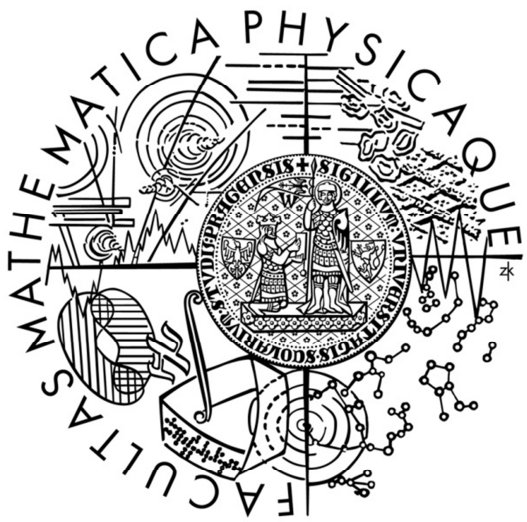

Bc. Daniel Duda

Visualization of selected flows of superfluid helium using solid hydrogen tracer particles

Department of Low Temperature Physics

Supervisor: prof. RNDr. Ladislav Skrbek, DrSc.

Consultant: Dr. Marco La Mantia, PhD.

Study programme: Physics

Specialization: Physics of Condensed Matter and Materials

Praha 2013

Zde vyslovuji poděkování svému vedoucímu, panu profesorovi RNDr. Ladislavu Skrbkovi, DrSc. za jeho příjemné vedení, za trpělivost při zodpovídání dotazů a za motivaci ke studiu právě tohoto oboru. Velmi děkuji svému konzultantovi Dr. Marcovi La Mantiovi, PhD. za jeho pomoc v mém krušném zápase s cizími jazyky, což ho stálo nemalé úsilí a nemálo času, neboť celou mou práci několikrát pročetl a opravil téměř každou větu. Největší poděkování náleží Bohu, stvořiteli uchvacující přírody, jejíž až závratně tajemnou nádheru a složitost můžeme zde na Matfyzu hledat, objevovat a studovat.

Prohlašuji, že jsem tuto diplomovou práci vypracoval samostatně a výhradně s použitím citovaných pramenů, literatury a dalších odborných zdrojů.

Beru na vědomí, že se na moji práci vztahují práva a povinnosti vyplývající ze zákona č. 121/2000 Sb., autorského zákona v platném znění, zejména skutečnost, že Univerzita Karlova v Praze má právo na uzavření licenční smlouvy o užití této práce jako školního díla podle § 60 odst. 1 autorského zákona.

V ..... dne .....

podpis

Název práce: Vizualizace vybraných proudění supratekutého hélia s využitím částic pevného vodíku

Autor: Bc. Daniel Duda

Katedra: Katedra fyziky nízkých teplot

Vedoucí diplomové práce: prof. RNDr. Ladislav Skrbek, DrSc, Katedra fyziky nízkých teplot, Matematicko-fyzikální fakulta Univerzity Karlovy v Praze.

Konsultant: Dr. Marco La Mantia, PhD.

Abstrakt: Práce se zabývá kvantovou turbulencí vytvářenou tepelným protiproudem normální a supratekuté složky v He II, která je studována na délkovém měřítku srovnatelném se vzdáleností mezi kvantovanými víry metodou sledování trasovacích částic pevného deuteria. Rozdělení podélných rychlostí vykazuje dvě maxima odpovídající dvěma rychlostním polím dvousložkového popisu He II. Rozdělení příčných rychlostí trasovacích částic při nízkých hodnotách připomíná klasické přibližně Gaussovské rozdělení, zatímco pro vyšší rychlosti má tvar mocninného rozdělení, což potvrzuje přítomnost kvantovaných vírů a tedy kvantovou povahu supratekutého hélia. Rozdělení zrychlení trasovacích částic se zdá být velmi podobné klasickému, alespoň ve studovaném rozsahu parametrů, avšak závislost velikosti zrychlení na teplotě a tepelném toku vytvářejícím tepelný protiproud může být vysvětlena na kvalitativní úrovni kvantovou povahou supratekutého hélia, vezmeme-li v úvahu poměr mezi viskózní silou způsobenou normální složkou supratekutého hélia a tlakovou silou vycházející z Bernoulliovy rovnice a působící na částici v blízkosti kvantovaného víru. Vizualizační metody se ukazují jako relevantní nástroj studia kvantové turbulence, k čemuž přispějí i připravované budoucí experimenty. V tomto smyslu jsou uvedeny také předběžné výsledky studia tepleného protiproudu v okolí válce.

Klíčová slova: Tepelný protiproud v supratekutém héliu 4, kvantová turbulence v supratekutém héliu 4, sledování trasovacích částic, rozdělení rychlostí, rozdělení zrychlení.

Thesis title: Visualization of selected flows of superfluid helium using solid hydrogen tracer particles

Author: Bc. Daniel Duda

Department: Department of Low Temperature Physics,

Supervisor: prof. RNDr. Ladislav Skrbek, DrSc, Department of Low Temperature Physics, Faculty of Mathematics and Physics, Charles University in Prague.

Consultant: Dr. Marco La Mantia, PhD.

Abstract: Quantum turbulence generated in thermal counterflow of He II is studied experimentally by visualization. The statistical properties of the motion of micron size solid deuterium particles are studied by using the particle tracking velocimetry technique at length scales comparable to the mean distance between quantized vortices. The probability density function (PDF) of the longitudinal velocity displays two peaks that correspond to two velocity fields of the two-fluid description of He II. The PDF of the transversal velocity displays a classical-like Gaussian core with non-classical power-law tails, confirming the quantum nature of turbulence in counterflowing He II. The distribution of the particle acceleration is found to be similar in shape to the classical one, in the range of investigated parameters. The observed dependencies of the average amplitude of the particle acceleration on the temperature and on the applied heat flux that generates the counterflow under study, are explained semi-quantitatively based on the quantum mechanical description of He II, by taking into account the ratio between viscous drag force of the normal component of He II and the Bernoulli pressure gradient force of superfluid component near the quantized vortices. Flow visualization is shown to be a valuable tool to study quantum turbulence and further investigations are under way. To this end, preliminary results on thermal counterflow past a cylinder are also discussed.

Keywords: Thermal counterflow in superfluid ^{4}He, quantum turbulence in superfluid ^{4}He, particle tracking velocimetry, probability density function of velocity, probability density function of acceleration.

Contents

Preface

For humans the most important sense is sight. Thus in order to discover the principles of Nature we prefer using it. Flow visualization is a very old method in its principle, but until the present "electronic age" it was not possible to use it for quantitative measurements. A lot of experiments have been performed in water or in air by using the tracer particles, carried by the fluid thanks to the viscous drag force, to visualize the flow. Now, quite exotic quantum liquids – the superfluid phases of ^{4}He or ^{3}He – are studied by contemporary visualization techniques.

The superfluid helium is a quantum liquid, displaying macroscopic quantum effects, where the quantized vortices exist and where totally different type of convection – the thermal counterflow – can be established and studied experimentally.

1. Theoretical introduction

1.1. Classical liquids

Equations of motion

If we have a volume filled with a classical liquid, we can divide such a volume into infinitesimally small volumes, and call them particles of liquid. The dynamics of such fluid particles can be modelled by the *Newton law*,

$$\frac{d\vec{p}}{dt} = \vec{f}, \tag{1.1}$$

where $\vec{p}$ is the momentum per unit volume and $\vec{f}$ denotes the force per unit of volume. As we implicitly assume that the considered fluid is a continuum, each quantity, A, which describes the properties of the liquid, is generally a function of space and time, that is, $A(\vec{r},t)$, where $\vec{r}$ is the distance from a generic point and t indicates the time. If A is a continuous quantity, it can be expressed in the form of a *Taylor polynomial*, i. e.

$$A\left(\vec{r}+\overrightarrow{\delta r}, t+\delta t\right) = A(\vec{r},t) + \overrightarrow{\delta r}\cdot\overrightarrow{\frac{\partial}{\partial r}}A(\vec{r},t) + \delta t\cdot\frac{\partial}{\partial t}A(\vec{r},t) + O(\delta r^2, \delta t^2).$$

It is possible to rewrite the left-hand side of equation (1.1) as

$$\frac{d\vec{p}}{dt} = \frac{\partial}{\partial t}\vec{p} + \frac{\partial\vec{r}}{\partial t}\cdot\overrightarrow{\frac{\partial}{\partial r}}\vec{p} = \frac{\partial}{\partial t}\vec{p} + (v\cdot\nabla)\vec{p}, \tag{1.2}$$

where the *momentum* $\vec{p}$ can also be expressed as

$$\vec{p} = \rho\cdot\vec{v},$$

where ρ is the *density* of the liquid and $\vec{v}$ indicates the *velocity* of a particle of liquid. These two quantities are related to each other by the *equation of continuity*, which is also called the *law of mass-conservation*. If, in a certain volume, the total amount of mass changes, it has to flow through the boundary Ω of the considered volume, i.e.,

$$\int_\Omega \frac{d\rho}{dt}dV = \int_{\partial\Omega}\rho\vec{v}\cdot\overrightarrow{dS}, \tag{1.3}$$

where V is the considered volume and $\vec{S}$ denotes the corresponding surface. By using the *Gauss-Ostrogratsky theorem*, i. e.,

$$\int_{\partial\Omega}\rho\vec{v}\cdot\overrightarrow{d\vec{S}} = \int_\Omega \nabla\cdot(\rho\vec{v})dV,$$

it is possible to integrate the right-hand side of (1.3) and obtain

$$\frac{d\rho}{dt} = \nabla\cdot(\rho\vec{v}) = \vec{v}\cdot(\nabla\rho) + \rho\nabla\cdot\vec{v}.$$

As ρ is a continuous quantity, its derivative can be expressed as

$$\frac{d\rho}{dt} = \frac{\partial\rho}{\partial t} + \vec{v}\cdot(\nabla\rho).$$

The *equation of continuity* can consequently be written as

$$\frac{d\rho}{dt} = \nabla\cdot(\rho\vec{v}) \text{ or } \frac{\partial\rho}{\partial t} = \rho\nabla\cdot\vec{v}. \tag{1.4}$$

The right-hand side of equation (1.1) depends on the physical situation under study. As a first step, the *Hook law* can be used to specify the force per unit of volume and (1.1) can be rewritten as

$$\frac{d\vec{p}}{dt} = \vec{f} = \vec{f}_{Hook} + \vec{f}_{other} = \nabla \cdot \sigma + \vec{f}_{other}, \tag{1.5}$$

where σ is a 2nd order tensor called *stress tensor*,

$$\sigma = \tau + \tau', \tag{1.6}$$

where τ' accounts for the contribution of the *viscosity* to σ, while τ is the pressure acting on the considered volume,

$$\tau_{ij} = -p\delta_{ij}.$$

In the case of *Newtonian fluids*, τ' is isotropic, homogenous and depends linearly on the *velocity of deformation*. For such a fluid it is possible to use the experimentally observed *Newton's law*,

$$\tau'_{ij} = \lambda\delta_{ij}\frac{\partial v_k}{\partial x_k} + \mu\left(\frac{\partial v_i}{\partial x_j} + \frac{\partial v_j}{\partial x_i}\right)_{i\neq j}, \tag{1.7}$$

where μ is the *dynamic viscosity* and λ indicates the *second viscosity*. This is possible as

$$\nabla\vec{v} = \nabla \cdot \vec{v} + \dot{e},$$

where $\dot{e}_{ij}$ is the *tensor of the velocity of deformation,* defined as

$$\dot{e}_{ij} = \frac{1}{2}\left(\frac{\partial v_i}{\partial x_j} + \frac{\partial v_j}{\partial x_i}\right)_{i\neq j}. \tag{1.8}$$

Each movement of the liquid, in the vicinity of a chosen fixed point x_j and at time t, can be decomposed into *translation*, *deformation* and *rotation*. The corresponding velocities are written as

$$v_i'(x_j + dx_j, t) = v_i(x_j, t) + \dot{e}_{ik}(x_k, t)dx_k + \dot{\omega}_{ik}(x_j, t)dx_k. \tag{1.9}$$

where $\dot{e}_{ij}$ is the just mentioned *tensor of the velocity of deformation*, and $\dot{\omega}_{ij}$ denotes the *tensor of the velocity of rotation*, defined as

$$\dot{\omega}_{ij} = \frac{1}{2}\left(\frac{\partial v_i}{\partial x_j} - \frac{\partial v_j}{\partial x_i}\right). \tag{1.10}$$

Equation (1.9) is called the *first Helmholtz theorem* and its proof can be found in [4].

Using formulae (1.1), (1.5), (1.6) and (1.7) we can write the *Navier-Stokes equation* for classical liquids as

$$\frac{dv_i}{dt} = -\frac{1}{\rho}\frac{\partial p}{\partial x_i} + \frac{1}{\rho}\left(\frac{\partial}{\partial x_i}\lambda\frac{\partial v_j}{\partial x_j} + \frac{\partial}{\partial x_j}\left(\mu\left(\frac{\partial v_i}{\partial x_j} + \frac{\partial v_j}{\partial x_i}\right)\right)\right) + \frac{1}{\rho}f_i, \tag{1.11}$$

or, in a vector form, as

$$\frac{d\vec{v}}{dt} = -\frac{1}{\rho}\nabla p + \frac{1}{\rho}\left(\nabla(\lambda\nabla \cdot \vec{v}) + \nabla \cdot (\mu\nabla\vec{v})\right) + \frac{1}{\rho}\vec{f},$$

where, similarly to equation (1.2),

$$\frac{d\vec{v}}{dt} = \frac{\partial\vec{v}}{\partial t} + \vec{v} \cdot \nabla\vec{v}. \tag{1.12}$$

In most cases it is possible to assume that the viscous coefficients λ and μ are space independent. Moreover, thanks to the equation of continuity (1.4), it is possible to neglect the term proportional to λ, if there is no way to change the density of the liquid or to generate mass (which can be opinable in the case of the normal component of superfluid helium). The *Navier-Stokes equation* (1.11) can then be expressed in the well-known form

$$\frac{d\vec{v}}{dt} = -\frac{1}{\rho}\nabla p + \frac{\mu}{\rho}\nabla^2\vec{v} + \frac{1}{\rho}\vec{f}, \tag{1.13}$$

where the *kinematic viscosity* $\nu = {}^{\mu}/_{\rho}$.

Reynolds number

It is possible to rewrite equation (1.13) by using the non-dimensional *Reynolds number*, *Re*, defined as

$$Re = \frac{V \cdot D}{\nu}, \tag{1.14}$$

where V and D are a typical *velocity* and *dimension* of the studied problem, respectively. The other quantities in (1.13) can consequently be nondimensionalized as $\vec{u} = {}^{\vec{v}}/_{V}$, $\vec{x} = {}^{\vec{r}}/_{D}$, $P = {}^{p}/_{\rho V^2}$, $\tau = {}^{Vt}/_{D}$ and $\overrightarrow{f'} = \frac{D}{\rho V^2}\vec{f}$. The *Navier-Stokes equation* can then be rewritten in a form that depends only on one parameter, the *Reynolds number*, as

$$\frac{\partial\vec{u}}{\partial\tau} + \vec{u}\cdot\nabla\vec{u} = -\nabla P + \frac{1}{Re}\nabla^2\vec{u} + \overrightarrow{f'}. \tag{1.15}$$

The *Reynolds number* can be seen as the ratio between inertial and viscous forces, i. e.

$$Re \approx \frac{\rho\frac{V^2}{D}}{\mu\frac{\partial^2 V}{\partial x^2}} \approx \frac{VD}{\nu}.$$

At small values of Re the viscous forces are dominant and the flow is generally laminar; at large values of Re the inertia of the liquid prevails and the flow may be turbulent.

Limits

Neglecting the viscous term, the second one of the right-hand side of (1.15), we obtain the *Euler equation* for inviscid ideal fluids

$$\frac{d\vec{u}}{d\tau} = -\nabla P + \overrightarrow{f'}. \tag{1.16}$$

Equation (1.16) looks like the *Navier-Stokes equation* at infinitely high *Reynolds number*, but it is not so, because the flow of a liquid with viscosity equal to zero is in general different from that of a liquid with very small but non-zero viscosity.

For a flow governed by the *Euler equation* (1.16) the non-linear second term of (1.12) is responsible for the occurrence of *chaotic behaviour*, rising from the fact that a *small* disturbance in the initial conditions produces *large* disturbances in a relatively short time. In general it is possible to write

$$\delta f(t) \approx e^{\lambda t} \cdot \delta f(0),$$

where the parameter λ is called the *Ljapunov exponent* (in Cyrillic *Ляпунов*, other transcriptions are *Lyapunov, Ljapunow* or *Liapunov*) and is typical for any system with *deterministic chaos*. In the case of linear evolution of the flow $\lambda = 0$, instead for turbulent flows generally $\lambda \neq 0$.

We obtain another interesting limit of the *Navier-Stokes equation* by neglecting the advective non-linear term in (1.12) and the externally applied force. Equation (1.15) then becomes

$$\frac{\partial \vec{u}}{\delta \tau} = -\nabla P + \frac{1}{Re}\nabla^2 \vec{u},$$

and is called the *diffusion equation*, with a pressure gradient force, for the three-dimensional variable $\vec{u}$; if we neglect the pressure gradient force, the equation has a simple solution of the form

$$u_i \approx e^{-\left(\tau + \sqrt{\frac{Re}{3}}\delta_{ij}x_j\right)}.$$

which shows the effect of the viscous force: it smooths each disturbance, instead of enhancing it.

1.2. Classical vortices

As mentioned above, the *first Helmholtz theorem* (1.9) states that each movement of the fluid in an infinitesimal neighbourhood of a chosen point is separable into *translation velocity* v_i, *velocity of deformation* $\dot{e}_{ik}$ and *velocity of rotation* $\dot{\omega}_{ik}$, that is

$$v_i'(x_j + dx_j, t) = v_i(x_j, t) + \dot{e}_{ik}(x_k, t)dx_k + \dot{\omega}_{ik}(x_j, t)dx_k.$$

The antisymmetric tensor $\dot{\omega}_{ij}$ can also be seen as a pseudovector of *rotation*,

$$\omega_i = \varepsilon_{ijk}\dot{\omega}_{jk} = \frac{1}{2}\varepsilon_{ijk}\left(\frac{\partial v_j}{\partial x_k} - \frac{\partial v_k}{\partial x_j}\right),$$

which is equal to the vector of *vorticity*, defined as

$$\omega_i = (\nabla \times \vec{v})_i = \varepsilon_{ijk}\frac{\partial v_j}{\partial x_k},$$

and its *divergence* is identically equal to zero,

$$\nabla \cdot (\nabla \times \vec{v}) = \frac{\partial}{\partial x_i}\varepsilon_{ijk}\frac{\partial v_j}{\partial x_k} = 0,$$

because the *derivation operator* is symmetric to exchanges between i and k, while the *Levi-Civita tensor* is antisymmetric.

It is possible to derive the *Navier-Stokes equation* for the *vorticity* by using the vector identity, known as "BAC - CAB",

$$u \times (\nabla \times u) = \nabla(u \cdot u) - (u \cdot \nabla)u,$$

and the advective term $(u \cdot \nabla)u$ of the *Navier-Stokes equation* can be rewritten as

$$(u \cdot \nabla)u = \frac{1}{2}\nabla|u^2| - u \times \omega.$$

By applying the *differential operator of rotation* on the *Navier-Stokes equation*, we then obtain

$$\frac{\partial \omega}{\partial \tau} + \nabla \times \left(\frac{1}{2}\nabla|u^2|\right) - \nabla \times (u \times \omega) = -\nabla \times (\nabla P) + \frac{1}{Re}\nabla^2 \omega,$$

where the operators $\frac{\partial}{\partial \tau}$ and ∇^2 were exchanged with $\nabla \times$, because they are partial differential operators. The terms containing the *rotation of gradient* are identically zero, because (as mentioned above) the *Levi-Civita tensor* is antisymmetric, while the partial derivation operator is symmetric to exchange of indices. Using the identity

$$\nabla \times (u \times \omega) = (u(\nabla \cdot \omega) - (u \cdot \nabla)\omega) - (\omega(\nabla \cdot u) - (\omega \cdot \nabla)u) =$$
$$= -(u \cdot \nabla)\omega + (\omega \cdot \nabla)u.$$

we finally obtain the *Navier-Stokes equation* for the *vorticity*, i. e.

$$\frac{\partial \omega}{\partial \tau} + (u \cdot \nabla)\omega - (\omega \cdot \nabla)u = \frac{1}{Re}\nabla^2 \omega,$$

or, similarly to equation (1.2),

$$\frac{d\omega}{d\tau} - (\omega \cdot \nabla)u = \frac{1}{Re}\nabla^2 \omega.$$

Second Helmholtz theorem

It is possible to express the *vorticity* ω as the limit of the *circulation* Γ along an infinitesimally short closed curve L, i. e.

$$\omega = lim_{L \to point}\, \Gamma_L = lim_{L \to point} \oint_L \vec{v} \cdot \overrightarrow{dl} \ ,$$

where, by using the *Stokes theorem*,

$$\Gamma_L = \oint_L \vec{v} \cdot \overrightarrow{dl} = \int_S (\nabla \times \vec{v}) \cdot \overrightarrow{dS} = \int_S \vec{\omega} \cdot \overrightarrow{dS} = \Gamma_S.$$

Here S is any surface bordered by the curve L.

The *Kelvin theorem* for the time evolution of Γ_L states that

$$\frac{d\Gamma_L}{dt} = \oint \frac{d\vec{v}}{dt} \cdot \overrightarrow{dl} + \oint \vec{v} \cdot \frac{d\,\overrightarrow{dl}}{dt},$$

where, if the curve L bounds a *simply connected region*,

$$\oint \vec{v} \cdot \frac{d\,\overrightarrow{dl}}{dt} = \oint \vec{v} \cdot \nabla\vec{v} \cdot \overrightarrow{dl} = \frac{1}{2}\oint (\nabla v^2) \cdot \overrightarrow{dl} = \frac{1}{2}\oint \left(\frac{\partial}{\partial x_i} v^2\right) \cdot dx_i = \frac{1}{2}\oint dv^2 = 0,$$

The time derivative of Γ_L is then the line integral of the *acceleration*, i. e.

$$\frac{d\Gamma_L}{dt} = \oint \frac{d\vec{v}}{dt} \cdot \overrightarrow{dl}.$$

By using the *Navier-Stokes equation* (1.15) and considering that the additional forces have a *potential* U,

$$\frac{d\Gamma_L}{dt} = \oint \frac{d\vec{v}}{dt} \cdot \overrightarrow{dl} = \oint \left(-\frac{1}{\rho}\nabla p + \frac{\mu}{\rho}\nabla^2 \vec{v} + \frac{1}{\rho}\nabla U\right) \cdot \overrightarrow{dl},$$

and, by using the *Stokes theorem*,

$$\frac{d\Gamma_S}{dt} = \int \left(-\frac{1}{\rho}\nabla \times (\nabla p - \nabla U) + \nu\nabla^2(\nabla \times \vec{v})\right) \cdot \overrightarrow{dS} = \int \nu(\nabla^2 \vec{\omega}) \cdot \overrightarrow{dS} \ .$$

The latter is equal to zero in the case of inviscid fluids ($\nu = 0$). Applying the limit to a small surface we obtain the *second Helmholtz theorem on the conservation of rotation for inviscid fluids*, i. e.

$$\frac{d\vec{\omega}}{dt} = 0. \tag{1.17}$$

This is very important for the properties of *quantized vortices* in a *superfluid*, because it predicts that, if a quantized vortex has in one point a certain value of circulation, it must have the same value along its entire length; see below.

1.3. Helium

Helium was discovered in 1868 in the spectral decomposition of the sunlight as an element not previously known. It was called *hélium* from the word *ó ἥλιος*, which means *the sun* in Greek.

Although helium is the second most common element in the Universe (after hydrogen), it is rare on Earth, because, being inert, does not form any solid or liquid compounds, and, being the second lightest gas, it goes up to the upper atmosphere, where is blown away by the solar wind.

Helium exists in the form of 2 stable isotopes, ^{3}He and ^{4}He, containing in the core 2 protons and 1 neutron, ^{3}He, and 2 neutrons, ^{4}He, respectively. In the shell it has 2 electrons filling the orbital *1s*, thus in this system there are 5, ^{3}He, or 6 particles, ^{4}He, with spin. The total absolute value of spin is then $\frac{1}{2}$, ^{3}He, or 0, ^{4}He, (considering no excitations) and the system of helium atoms is consequently governed by the *Fermi-Dirac statistic*, ^{3}He, or by the *Bose-Einstein statistic*, ^{4}He, which are

$$f_{FD}(E,T) = \frac{1}{e^{\frac{E-\mu}{k_B T}} + 1}, \tag{1.18}$$

and

$$f_{BE}(E,T) = \frac{1}{e^{\frac{E-\mu}{k_B T}} - 1}, \tag{1.19}$$

respectively; where μ indicates the *chemical potential* and k_B is the *Boltzmann constant*. These different statistical distributions are responsible for the fact that ^{3}He and ^{4}He have different properties at low temperatures, although at high temperatures they are very similar, because the high temperature limit of both statistics is the *Boltzmann statistics.*

Both isotopes do not form the solid state, at atmospheric pressure, until the temperature reaches the absolute zero; both become liquid at few Kelvin, 4,215 K for ^{4}He and 3,19 K for ^{3}He, [1], and both have the *superfluid phase,* which is however generated by different mechanisms. The isotope ^{4}He has the transition to the *superfluid phase*, called *λ-transition*, at the temperature $T_\lambda = 2{,}1768$ K, at the saturated vapour pressure [2], while ^{3}He, being a *fermion*, must form *Cooper pairs*, which have an integer absolute value of spin (equal to one). Its superfluid transition temperature is 1000 times lower, 0,93 mK, at the saturated vapour pressure [1].

^{4}He is obtained by the α-decay of heavy metals, such as uranium and thorium, or by the fractional distillation of *natural gas* (which usually contains CH_4, C_2H_6, other hydrocarbonates and gases, such as N_2, CO_2 and He).

^{3}He is instead the product of the decay of *tritium*, which mostly occurs in thermonuclear weapons,

$$^3_1H \rightarrow {}^3_2He^+ + e^- + \overline{\nu}_e,$$

and, having a large cross section for trapping neutrons, is industrially used for neutron detectors.

In this work only the ^{4}He isotope will be studied.

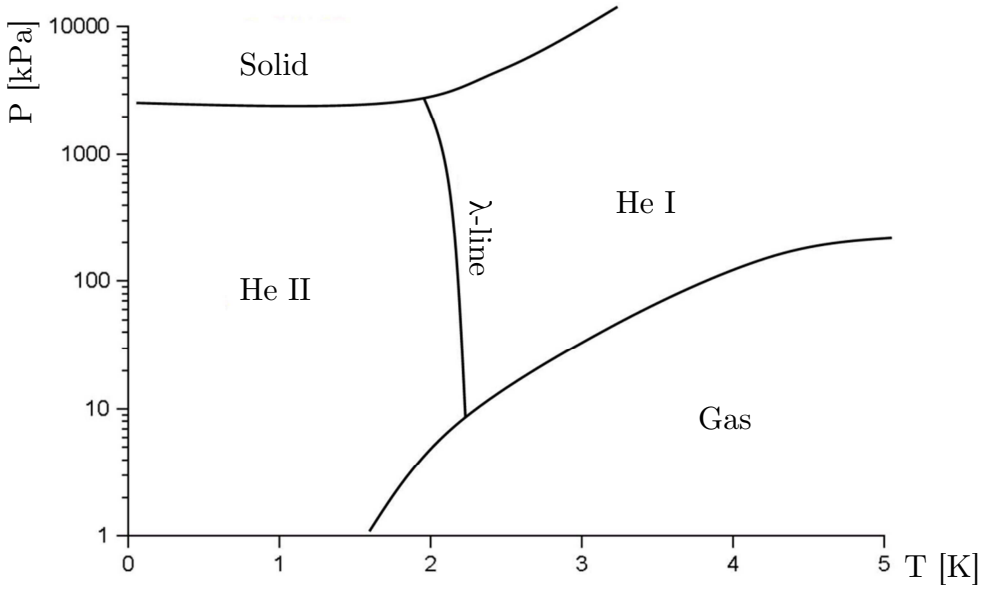

Figure 1.1 *Equilibrium phase diagram of ^{4}He with temperature on the horizontal axis and pressure on the vertical axis* [1].

In the helium's phase diagram there is not the *Triple point* while the *Critical point* has temperature $T_C \cong 5{,}2\,K$ and pressure $p_C \cong 226\,kPa$ [1]. The transitions between liquid, gas and solid are phase transitions of *first order*. The transition between He I and He II is instead a transition of *second order*; there is no *latent heat* and consequently He I and He II do not coexist.

He I is a classical liquid with very low and wide ranging values of the *kinematic viscosity*, at 2,25 K it has for example a viscosity ν equal to $1{,}96 \cdot 10^{-4}$ cm^2s^{-1} [1], which is about three orders of magnitude smaller than the kinematic viscosity of air.

1.4. Superfluid helium

He II is a quantum liquid, described by various theories, such as the *Bose-Einstein condensation theory*, Tizsa's and Landau's *two-fluid-models*, the latter based on phenomenological description of phonon dispersion relation, [1].

The fact that He is a quantum liquid means that its *de Broglie wavelength* is comparable with the distance between atoms. Their *wave functions* consequently overlap and we can define a macroscopic wave function ψ and write the corresponding *Schrödinger equation*,

$$i\hbar\frac{\partial}{\partial t}\psi = -\frac{\hbar^2}{2m}\Delta^2\psi + U\psi, \tag{1.20}$$

where we can ignore the fast changing microscopic contribution to the potential U and write it as a *chemical potential* μ.

The macroscopic wave function ψ has *magnitude* ψ_0 and *phase* φ,

$$\psi = \psi_0 e^{i\varphi}, \tag{1.21}$$

where the square of ψ_0 is proportional to the *density of the superfluid component*, $\psi_0 = \sqrt{\rho_s}$. It is also possible to consider the latter homogenous and stationary. By applying the *impulse operator* $\hat{p}$ on ψ we obtain

$$\hat{p}\psi = -i\hbar\nabla\sqrt{\rho_s}e^{i\varphi} = \hbar(\nabla\varphi)\sqrt{\rho_s}e^{i\varphi},$$

and, consequently

$$\vec{p} = \hbar\nabla\varphi \text{ and } \vec{v} = \frac{\hbar}{m}\nabla\varphi. \tag{1.22}$$

The velocity field is *potential* and its circulation is zero in a simple connected fluid region, because the *circulation operator* is antisymmetric, while the *gradient* is symmetric.

Using (1.22) and (1.21) in the *Schrödinger equation* (1.20) we obtain

$$i\hbar\cdot\sqrt{\rho_s}e^{i\varphi}\cdot i\frac{\partial\varphi}{\partial t} = -\frac{\hbar^2}{2m}\cdot\sqrt{\rho_s}e^{i\varphi}\cdot((i\nabla\varphi)^2 + i\Delta\varphi) + U\cdot\sqrt{\rho_s}e^{i\varphi},$$

which, after dividing by $\sqrt{\rho_s}e^{i\varphi}$, is separable into *real* and *imaginary* parts, i. e.

$$-\hbar\frac{\partial\varphi}{\partial t} = \frac{\hbar^2}{2m}(\nabla\varphi)^2 + U \text{ and } \Delta\varphi = 0. \tag{1.23}$$

The imaginary part of (1.23) is similar to the *continuity equation* (1.4), without the time derivative of the density, as assumed above. By applying the *gradient operator* to the real part of (1.23) we obtain

$$-\hbar\frac{\partial}{\partial t}\nabla\varphi = \frac{\hbar^2}{2m}\nabla(\nabla\varphi)^2 + \nabla U,$$
$$-m\frac{\partial}{\partial t}v = \frac{m}{2}\nabla v^2 + \nabla U = m\cdot v\cdot\nabla v + \nabla U,$$

which has the form of the *Euler equation*

$$\frac{\partial}{\partial t}v + v\cdot\nabla v = -\frac{1}{m}\nabla U, \tag{1.24}$$

where the *potential* U has in this case, according to [8], gradient

$$\nabla U = \frac{m}{\rho}\nabla p - s\nabla T - \frac{\rho_n}{2\rho}\nabla(\overrightarrow{v_n} - \overrightarrow{v_s})^2,$$

where T is the *thermodynamical temperature*, p indicates the *pressure* and s denotes the *specific entropy*, ϱ_n and ϱ_s are the *densities* of the *superfluid* and *normal fluid* components, respectively, and $\overrightarrow{v_n}$ and $\overrightarrow{v_s}$ indicate the corresponding velocities.

From (1.24) we then obtain the *equation of motion* for the *superfluid* component of He II, that is

$$\rho_s \frac{\partial}{\partial t}\overrightarrow{v_s} + \rho_s \overrightarrow{v_s} \cdot \nabla \overrightarrow{v_s} = -\frac{\rho_s}{\rho}\nabla p + \rho_s s \nabla T + \frac{\rho_s \rho_n}{2\rho}\nabla(\overrightarrow{v_n} - \overrightarrow{v_s})^2. \qquad 1.25$$

From the *equation of continuity* (1.4) we instead obtain the *equation of motion* for the *normal* component, i. e.

$$\rho_n \frac{\partial}{\partial t}\overrightarrow{v_n} + \rho_n \overrightarrow{v_n} \cdot \nabla \overrightarrow{v_n} = -\frac{\rho_n}{\rho}\nabla p - \rho_n s \nabla T - \frac{\rho_s \rho_n}{2\rho}\nabla(\overrightarrow{v_n} - \overrightarrow{v_s})^2 + \nu \Delta \overrightarrow{v_n}, \qquad 1.26$$

where the density of the liquid is the sum of the densities of the *normal* and *superfluid* components,

$$\rho = \rho_s + \rho_n, \qquad 1.27$$

the *density of momentum per unit volume* $\vec{j}$ being defined as

$$\vec{j} = \rho_s \overrightarrow{v_s} + \rho_n \overrightarrow{v_s}, \qquad 1.28$$

and ν is the *kinematic viscosity* of the *normal* component.

Quantized vortices

According to (1.22) the circulation of the *superfluid* velocity v_s is zero, where the macroscopic wave function ψ exists. If there is any point inside the region filled by He II where the density of the *superfluid* component is zero, the circulation can there be non-zero and its value is restricted by the quantum nature of He II.

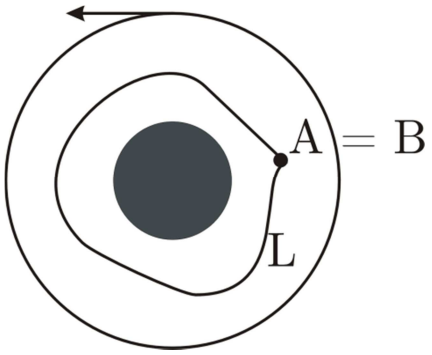

Figure 1.2 *Closed curve L around any region without the superfluid component; its initial point is called A and its final point B.*

As the wave function ψ has to be unambiguous, it has the same value at the generic points A and B on Figure 1.2, if these points are identical, i. e.

$$\psi(A) = \psi(B),$$

where, according to (1.21),

$$\psi(A) = \sqrt{\rho_s} e^{i\varphi(A)} = \psi(B) = \sqrt{\rho_s} e^{i\varphi(B)}.$$

As the *exponential function* of the imaginary argument is 2π-periodic, we obtain

$$\varphi(A) = \varphi(B) + 2\pi n,$$

where $n \in \mathbb{N} \cup \{0\}$. The circulation along curve L can then be rewritten as

$$\Gamma_L = \oint_L \overrightarrow{v_s} \cdot \overrightarrow{dl} = \oint_L \frac{\hbar}{m}\nabla\varphi \cdot \overrightarrow{dl} = 2\pi n \frac{\hbar}{m} = n\kappa, \qquad 1.29$$

where κ is the *quantum of circulation*,

$$\kappa = \frac{h}{m_{^4He}} \approx 10^{-7} m^2 s^{-1} \text{ [1]}. \tag{1.30}$$

As the circulation is quantized, the vortex has the same circulation along its length. Besides, a vortex (as mentioned above) cannot begin free in the liquid but has to be attached to its boundaries, i. e., the free surface or the walls, or can form a closed loop (Figure 1.3).

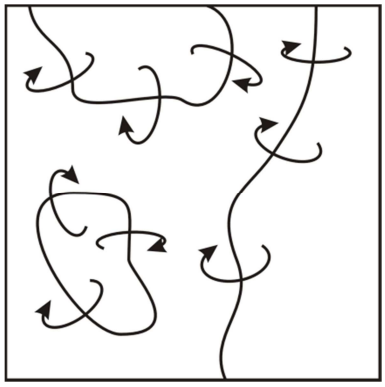

Figure 1.3 *Quantized vortex can only be attached to the free surface or volume walls or can form a closed loop.*

The phase φ of the wave function ψ can be seen as an angle, in polar coordinates, in a plane perpendicular to the vortex. Equation (1.23) can consequently be rewritten as

$$\Delta\varphi = \nabla \cdot \nabla\varphi = \nabla \cdot \left(\nabla n \cdot arctg\left(\frac{x}{y}\right)\right) = n\,\nabla \cdot \left(\frac{y}{x^2+y^2}, -\frac{x}{x^2+y^2}\right) = 0$$

for $x \neq 0$ and $y \neq 0$. The *superfluid* velocity v_s in a plane perpendicular to the vortex line results

$$\overrightarrow{v_s}^{2D} = \frac{\hbar}{m}\nabla\varphi = n\frac{\hbar}{m}\left(\frac{y}{x^2+y^2}, -\frac{x}{x^2+y^2}\right), \tag{1.31}$$

and its *rotation* is equal to zero everywhere except at the origin (0, 0)

$$\nabla \times \overrightarrow{v_s}^{2D} = n\frac{\hbar}{m}\nabla \times \left(\frac{y}{x^2+y^2}, -\frac{x}{x^2+y^2}\right) = 0.$$

The *energy* of a vortex line, per unit of length, can be calculated as the kinetic energy of the orbiting *superfluid* component, i. e.

$$\frac{dE}{dl} = \oint \int_a \frac{1}{2}\rho_s v_s^2\, r\, dr\, d\alpha = \frac{1}{2}\rho_s n^2 \frac{\hbar^2}{m^2} \oint \int_a \frac{1}{r} dr\, d\alpha = \pi\rho_s n^2 \frac{\hbar^2}{m^2} \ln\left(\frac{b}{a}\right) = n^2 \cdot \frac{dE_1}{dl}, \tag{1.32}$$

where a is the radius of the vortex core given by the *coherence length* and b indicates the upper limit of the integration that corresponds to the mean distance between vortices. We can see that the energy of a vortex is proportional to n^2. It is therefore energetically advantageous to split one multiply quantized vortex line into single vortex lines.

Thermal counterflow

By comparing equations (1.25) and (1.26) we see that the terms with thermal gradient have different signs for the *normal* and *superfluid* components of He II. The gradient of temperature drags consequently each component in opposite directions and this is the origin of the *thermal counterflow*.

In He II only the *normal* component carries the entropy because the *superfluid* component is in the ground state. The *normal* component can then be seen as the gas of thermal excitations [1]. The heat transfer q is obtained by the formula

$$q = \rho s T v_n, \tag{1.33}$$

where T is the *temperature* of the helium bath, s denotes the *specific entropy* and ϱ indicates the fluid *density*. From the *continuity equation* it is possible to determine the velocity of the *superfluid* component as

$$v_s = -\frac{\rho_n}{\rho_s} v_n.$$

Thermal counterflow can generate *quantum turbulence*, because, according to [1] the *mutual friction term* F_{sn}, which was introduced for the first time by Vinen [13], is added to equations (1.25) and (1.26). The formula for F_{sn} was derived from experiments on the attenuation of *second sound* in a cryostat rotating with angular velocity Ω and can be written as

$$F_{sn} = B\frac{\rho_s\rho_n}{\rho}\frac{1}{|\Omega|}\vec{\Omega}\times\left(\vec{\Omega}\times(\langle\overrightarrow{v_s}\rangle - \langle\overrightarrow{v_n}\rangle)\right) + B'\frac{\rho_s\rho_n}{\rho}\vec{\Omega}\times(\langle\overrightarrow{v_s}\rangle - \langle\overrightarrow{v_n}\rangle), \tag{1.34}$$

where B and B' are experimentally observed parameters; $\langle\overrightarrow{v_s}\rangle$ and $\langle\overrightarrow{v_n}\rangle$ indicate the velocities of the *normal* and *superfuid* components averaged over an area where there are enough vortices.

1.5. Particle tracking velocimetry technique

Particle tracking velocimetry (PTV) is a visualization technique that can be seen as belonging to the larger set of PIV (particle imaging velocimetry) techniques. To visualize the motion of a fluid, which is typically transparent, a number of opaque particles, called tracers, are added to the fluid and follow thus its motion, making it visible.

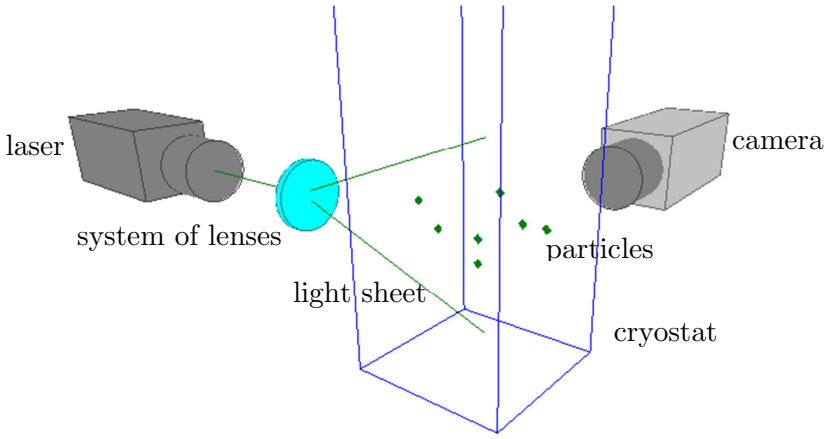

Figure 1.4 *Sketch of a typical PIV apparatus. The moving particles are illuminated by a laser and their time-dependent positions recorded by a camera, placed perpendicularly to the light sheet.*

More specifically, PIV methods are based on searching the local maximum in a *pair distribution function* with shift defined as

$$g_A(\vec{\rho}) = \sum_{\vec{r}\in A} I(\vec{r},t)\cdot I(\vec{r}+\vec{\rho},t+\Delta t), \qquad 1.35$$

where $I(r,t)$ is the light intensity of the considered images as a function of position r and time t. Purpose-made algorithms are then used to find the $\overrightarrow{\rho_A^*}$ that satisfies $g_A(\overrightarrow{\rho_A^*}) = \max\{g_A(\vec{\rho})\}$. The velocity of a group of particles in a certain area A, subset of the whole image, is consequently obtained as

$$\overrightarrow{v_A}(t) = \frac{\overrightarrow{\rho_A^*}}{\Delta t}.$$

Δt being the time between frames. This method, frequently used in classical fluid mechanics laboratories, corresponds to the *Euler's point of view* and gives information about the entire flow field, with a space-resolution equal to the size of the mentioned subset A. In our case it is not suitable to use it, mostly because, as mentioned above, there are two flows and consequently two „types of behaviour" of tracers, one carried the by *normal component* of the liquid and the other trapped into the *quantized vortex cores*.

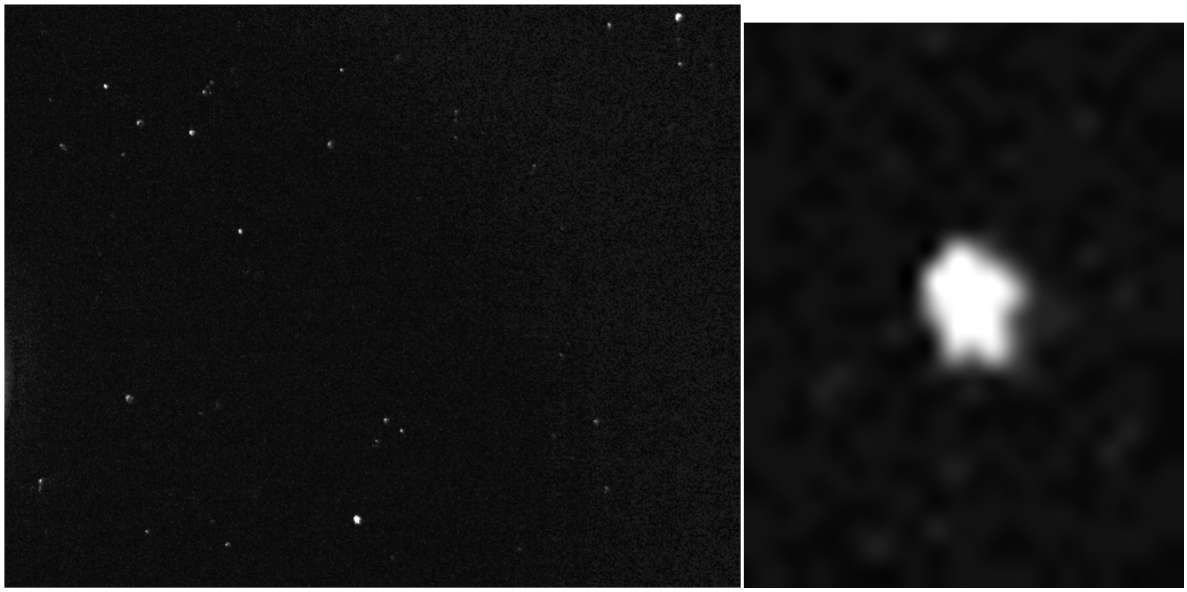

Figure 1.5 *Sample images with tracers. Left: field of view of the size 6 × 4 cm. Right: zoom of one particle.*

The PTV method is based on following individual particles. Purpose-made algorithms find in each image the particles, recorded as clusters of white pixels on a black background. Once this is done, other procedures connect the found particles to form trajectories.

This method corresponds to the *Lagrange's point of view* and is deemed to give information on the motion of individual particles of fluid. It does not generally correspond to the *Euler's viewpoint*, which instead looks at the fluid motion at specific locations. In the limit of *steady flow* this two points of view are equivalent.

The mentioned techniques are based on following particles carried by the fluid, and lay on the assumption that such particles follow closely the motion of the liquid.

In the case of the *normal component* of He II, which is assumed to be a classical fluid, tracer particles follow the fluid flow as in classical fluids due to the fluid viscosity. In the case of the *superfluid component* of He II, which is defined as an inviscid fluid, the *D'Alembert's paradox* applies. The latter states that

$$\vec{v} \cdot \vec{F} = 0,$$

where $\vec{v}$. is the velocity of a moving body relative to the fluid and $\vec{F}$ is the force acting on the body. However, the force due to the gradient of pressure in the vicinity of vortex cores or other sharp boundaries still exists.

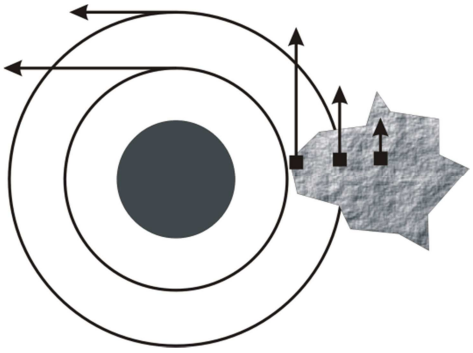

Figure 1.6 *Particle near a vortex core. Not to scale – the quantized vortex core diameter is of the order of Å [1]; particle diameter is instead of few μm, see Figure 2.7 below.*

Figure 1.6 shows a particle near the vortex core. In the flow around the particle a gradient of the square of the velocity exists. The latter corresponds to the gradient of pressure due to the *law of energy conservation*, which, for an incompressible inviscid fluid, is known as the *Bernoulli equation*, see for example [4], and [16], and generally reads

$$\frac{1}{2}u^2 + P + U = Const., \tag{1.36}$$

where u is the fluid *velocity*, P denotes the corresponding *pressure*, U represents the potential energy and *Const.* indicates an integration constant generally different for each streamline.

The detailed mechanism of particle trapping is not entirely understood due to number of effects affecting the interaction between vortices and particles. The trapping depends in classical fluids on the density of particle [16]; the heavier particle is repulsed from the vortex due to inertia, while the lighter particle is attracted due to the just described mechanism.

The experiments in the He II, which use as tracers the positive or negative ions of helium atom, show that the trapping does not depend on the density of particles in He II, [31], as the positive ions have larger density than He II, while the negative ions have just the additional hydrodynamic mass and thus have smaller density.

The energy of quantized vortex line can be expressed as the kinetic energy of *superfluid component* of He II orbiting the quantized vortex core, see equation (1.32). The passing of the vortex core through the particle is energetically favourable and the particle can be trapped on the vortex core. The latter depends on the previous velocity of particle and on the drag force due to the *normal component* of He II acting on the particle. The dissipative mechanisms, reducing the kinetic energy of particle moving relatively to the vortex core and thus enabling the trapping, are not entirely understood [1]. In the experiment, it is not possible to determine, if one particle is trapped or not.

2. Experimental setup

2.1. Cryostat

In order to keep helium in the liquid phase (see Figure 1.1) a cryostat, i. e. a good thermal insulating vessel, is needed. In our laboratory we use a cryostat with 5 optical ports: it was designed at MFF UK and assembled by Precision Cryogenic Systems. This device is well described in the previous work of my colleagues [14].

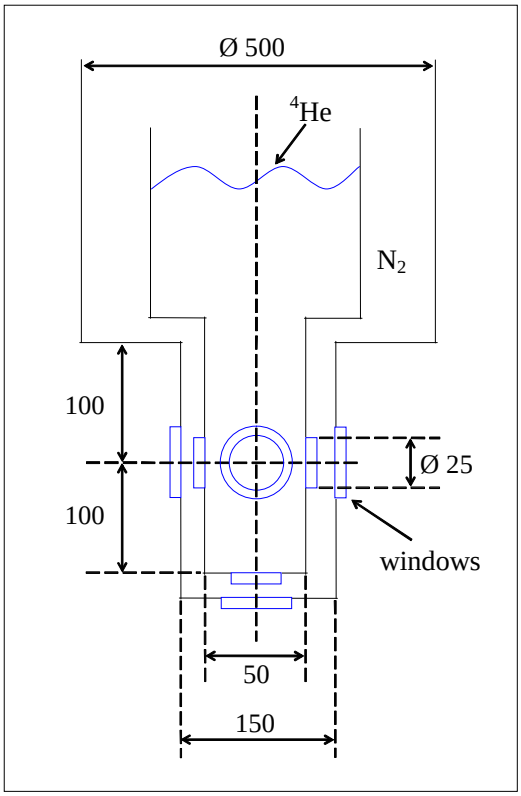

Figure 2.1 *Sketch of the optical tail of the cryostat, dimensions are in mm, [14].*

The cryostat can store more than 50 l of liquid helium, which is enough for an experimental run. It is usually not refilled during the experiment as this would most likely decrease the images quality by increasing the number of spurious particles. Care is indeed taken to ensure that the helium is as clean as possible, by flushing the cryostat with purified helium gas, before each experiment.

The inner volume of the cryostat is thermally shielded by a cylindrical volume of liquid nitrogen, as this reduces the *radiant* component of heat flow according to the *Stefan-Boltzmann law*, $P \approx \Delta T^4$. There is also another volume (not shown in Figure 2.1), which is evacuated and thus reduces thermal *conduction*. This volume is regularly pumped before each experiment, keeping the pressure in it typically between 1 and $3 \cdot 10^{-5}$ Torr.

There are 3 windows for each of the 5 optical ports (not only 2, as shown in Figure 2.1); the innermost windows are made of sapphire, while the others are made of quartz.

The cross-section of the optical tail is square with side of 50 mm (see Figure 2.1), while the largest part of the cryostat has a cylindrical shape with inner diameter equal to 200 mm. The windows have circular cross-section with diameter equal to 25 mm.

2.2. Pumping system

After liquid helium is transferred into the cryostat the helium bath has a temperature of 4,2 K, which is the boiling temperature of helium at atmospheric pressure. To decrease the temperature we decrease the bath pressure along the curve of *saturated vapour pressure* (see Figure 1.1), which is also used for measuring the temperature, see my previous work [10].

In order to do so we use two pumps connected in series: the first one is a Roots pump, with maximum pumping rate of 324 m^3/h, while the other is a mechanical rotary pump, with a maximum pumping rate of 36 m^3/h. Between them is a butterfly valve with a bypass. The automatic electronic control unit at higher pressures switches on the rotary pump only, at lower pressures adds the Roots pump.

The pumping unit is connected to the cryostat via a bellows tube of 50 mm diameter. The vibrations produced by the pumps are also reduced by a purpose-made bellows T-piece. To avoid spurious electrical currents the bellows tube is insulated from the cryostat by a plastic o-ring.

The output of the pumps is led into the He return line or into the open air, depending on the situation (cooling down the helium bath, belongs to the first case, evacuating the cryostat, to the latter case).

2.3. Thermometry

As the main thermometer in this experimental setup, as mentioned above, serves the saturated vapour pressure curve. The latter is used to define the temperature T between 1,25 K and 5,0 K, as reported by the norm ITS-90 [2], by using the formula

$$T = A_0 + \sum_{k=1}^{9} A_k \left(\frac{\ln p - B}{C}\right)^k, \qquad 2.1$$

where p is the pressure, while A_k, B and C are coefficients defined in [2]. The saturated vapour pressure versus temperature dependence is shown in Figure 2.2.

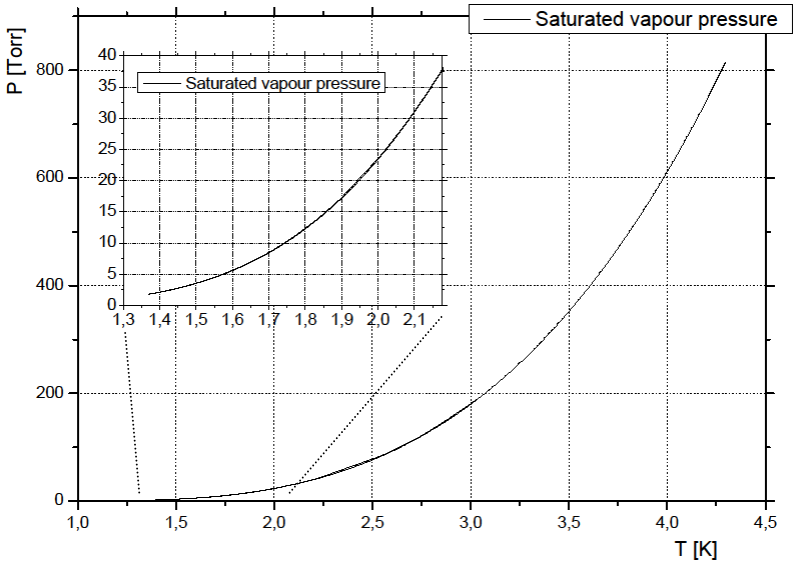

Figure 2.2 *Saturated vapour pressure of ^{4}He as a function of temperature. Inset: saturated vapour pressure in the range of He II, i. e. below the λ-temperature.*

The measurement of temperature was the topic of my Bachelor Thesis [10]. On the enclosed CD there is also a program I developed to calculate the temperature from the measured pressure.

As secondary thermometers a pair of semiconductor resistors is used. These are located inside the bath: the first one is on the flange placed just above the tail, the second one is placed closer to the main experimental volume, inside the tail. The resistance is measured by the 4-point method, see below, and converted to temperature by using relevant tabulated coefficients.

2.4. Measurement of pressure

The temperature was obtained from equation (2.1) by using the measured *saturated vapour pressure* of the bath of liquid helium. The pressure was measured by a *Baratron MKS 690A* sensor connected to the cryostat by a capillary of 8 mm inner diameter. It is assumed that the measured pressure is not affected by the state of helium gas in the tube. The difference in height between the sensor and level of liquid helium in the cryostat is around 80 cm. The level of liquid helium is however changing during the experiment, as the temperature is lowered by pumping the vapour, thus reducing the amount of liquid helium inside of cryostat. The difference in height of the level of liquid helium is deemed not to affect significantly the measured pressure due to the low density of gaseous helium, which is about 1,2 kg/m^3 [5].

According to the manufacturer the used sensor measures the pressure absolutely. It is connected to the *signal conditioner MKS 670*, which communicates with the computer via a GPIB bus.

The pressure is usually measured in *Torr* („millimetre of mercury column“, 1 Torr = 133,322 Pa) and in these units it will be presented below.

2.5. Measurement of resistance

As mentioned above, two semiconductor resistors are also used for temperature measurements. One of them is the resistor III B used in my Bachelor thesis [10]. It is a RuO_2 resistor and its room temperature resistance is around 1580 Ω. In order to obtain the temperature, the calibration discussed in [10] was used. The second one is a mass carbon TVO resistor with tabulated values of temperature and resistance. Its room temperature resistance is around 918 Ω.

For the measurements the 4-point method, sketched in Figure 2.3, is used. It reduces the effect of current leads on the measurement and consequently enables the use of *manganine wires* (alloy of Cu, Mn and Ni). This is advantageous to reduce the heat flux into the cryostat, as manganine has lower thermal conductivity than Cu but has also lower electrical conductivity.

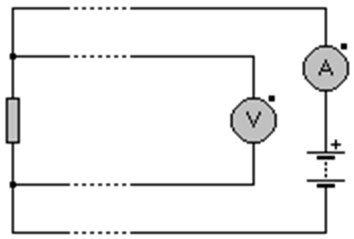

Figure 2.3 *Scheme of the 4-point method.*

The used power source was manufactured by Ing. František Soukup and is stable enough to avoid the need to measure the current. The used current is 1 mA but it is possible to switch the device to 0,1 mA or 10 mA, depending on what is needed, lower noise or lower overheating. The voltage is measured by the shielded unit NI SCB-68, which enables measurement of multiple signals and is connected to one of the computers used for the data collection and processing.

2.6. Heater

As mentioned in section 1.4, *thermal counterflow* is generated by heating the helium bath and causes the two components of He II to flow in opposite directions, to conserve the liquid helium mass. To generate such a heat flux we used two plane square heaters, made of lead in a thin kapton layer. In the first experiments a heater of 50 mm sides was used and placed on the bottom of the cryostat tail. This was later replaced by a smaller heater, of 25 mm sides, placed on the bottom of a suitably sized channel, inserted in the tail.

A MOTECH programmable DC power supply is used for the heater. The electrical scheme is similar to that shown in Figure 2.3. To measure the current and voltage, two Keithley multimeters are used. The latter and the power supply are connected to the computer by using a GPIB bus.

The room temperature resistance of the heaters is around 73 Ω and; at low temperatures it is very similar, about 72 Ω.

The main reason that justifies the measurement of the applied power, instead of just setting the latter on the power supply, is that a sizeable portion of the supplied power is dissipated in the circuit wires.

To connect the heaters to the power supply and to the multimeters copper wires are used, as they have larger electrical conductivity than manganine wires (the heat conductivity is larger too, according to the *Wiedemann-Franz Law*).

2.7. Experimental cell

As mentioned above, in the tail of the cryostat, sketched in Figure 2.1, we have also inserted, in a number of experiments, a smaller experimental cell with inner square section of 25 mm sides and inner height of 95 mm, see Figure 2.4. The cell vertical sides are removable glass plates of suitable dimensions. The columns and bases were manufactured of brass and painted black to avoid reflections.

Figure 2.4 *Photograph of the experimental cell. The shown cylinder was used for a series of experiments (see below) and can be removed.*

The main reason that justifies the use of the just described cell is to increase the local density of particles and to contain the production of classical convection structures, which are, naturally, not prohibited in quantum liquids.

2.8. Seeding system

As liquid helium is a colourless and transparent substance, to visualise its motion small flow tracers are added to it. For this purpose we use solid hydrogen and

deuterium particles, which are generally of sizes of few μm (see Figure 2.6). To obtain these particles we inject a mixture of helium, hydrogen and deuterium gases into the bath at a pressure larger than that of the bath.

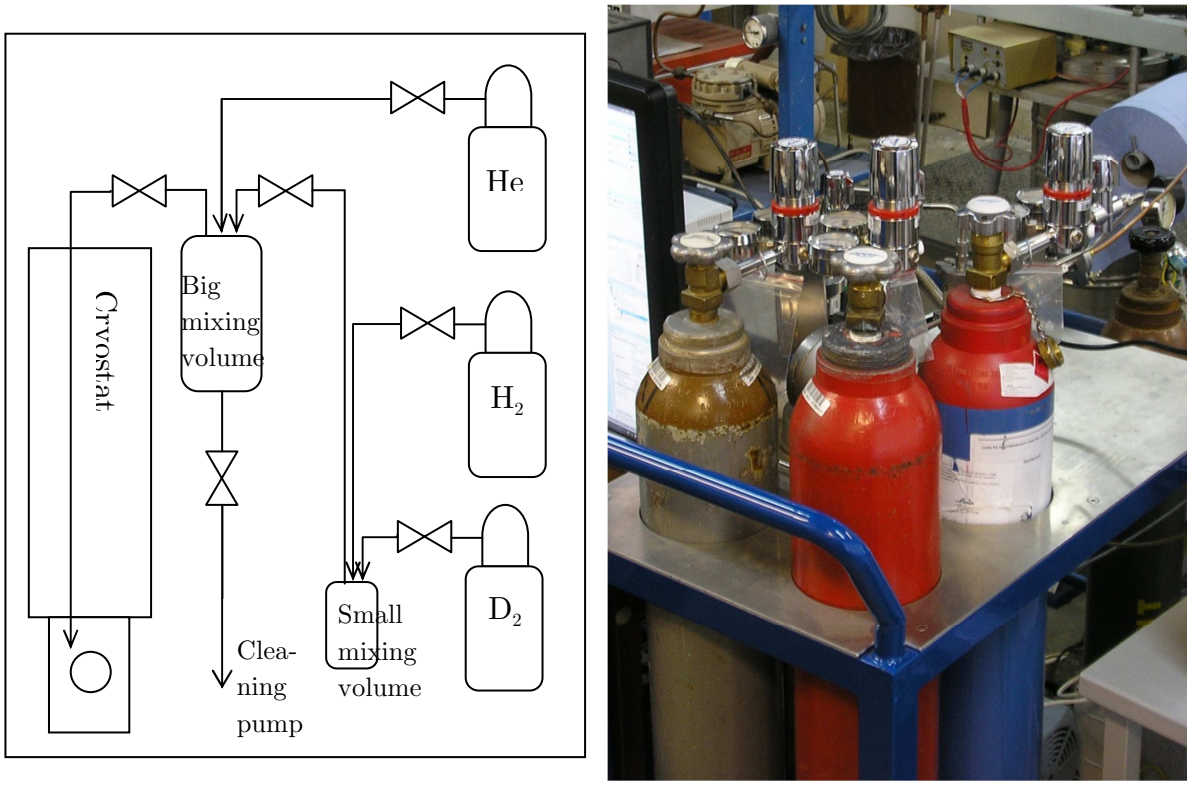

Figure 2.5 *Seeding system; left: sketch; right: photograph. On the sketch the pressure regulators between each gas bottle and first valve are not displayed. The last valve before the cryostat is computer-controllable and faster than the others. The big mixing volume is approximately 50 times larger than the small one. The tubes have outer diameter of 7 mm.*

As solid hydrogen has smaller density (88 kg·m^{-3} [35]) than that of liquid helium (146 kg·m^{-3} at temperatures between 1,0 and 2,5 K) and solid deuterium has larger density (200 kg·m^{-3} [35]), the initial idea was to mix this two isotopes to obtain particles with the same density of liquid helium. It was found that this is not possible due to the fact that hydrogen isotopes have different crystallization temperatures: particles made of hydrogen and particles made of deuterium were observed, as they have different settling velocities, and it does not seem that in the ranges of used parameters buoyant particles of suitable size can be obtained. Most experiments were later performed by using deuterium particles, as they appeared more suitable for our visualisation purposes.

On the seeding system metallic support, which is also equipped with wheels, there are three high-pressure gas bottles: the first one is filled with helium gas, the second one with hydrogen gas and the third one with deuterium gas, see Figure 2.5. In the small mixing volume it is possible to mix hydrogen and deuterium gases at various ratios. The obtained gaseous mixture is then diluted into the big mixing vol-

ume by using helium gas. This step is mainly needed to prevent the creation of a plug of solid mixture in the tube. The ratio of helium gas in the final mixture also affects the size of the obtained solid particles, together with other parameters, such as the mixture pressure and the injection velocity. Various combinations of these parameters were used and that yielding the most suitable sized particles used in the majority of experiments.

The size of the particles is calculated from their settlings velocities, assuming that the particles are spherical and that the *gravitational* force and *buoyancy* force are balanced by the *Stokes drag* force, due to the viscosity of the *normal component* of He II, i. e.

$$F_S = F_{vz} - F_g,$$
$$6\pi \cdot \mu \cdot R_p \cdot v = \frac{4}{3}\pi \cdot R_p^3 \cdot (\rho_{He} - \rho_p) \cdot g,$$

where μ is the dynamic viscosity of the *normal component* of He II, R_p indicates the radius of the particle and v denotes the settling velocity; ϱ_{He} is the *density* of helium, ϱ_p denotes the density of the particle and g indicates the acceleration due to gravity. The radius of the particle is finally obtained as

$$R_p = \sqrt{\frac{9 \cdot \eta \cdot v}{2 \cdot g \cdot (\rho_{He} - \rho_p)}}. \qquad 2.2$$

An example of distribution of particles radii calculated in this way is shown in Figure 2.6.

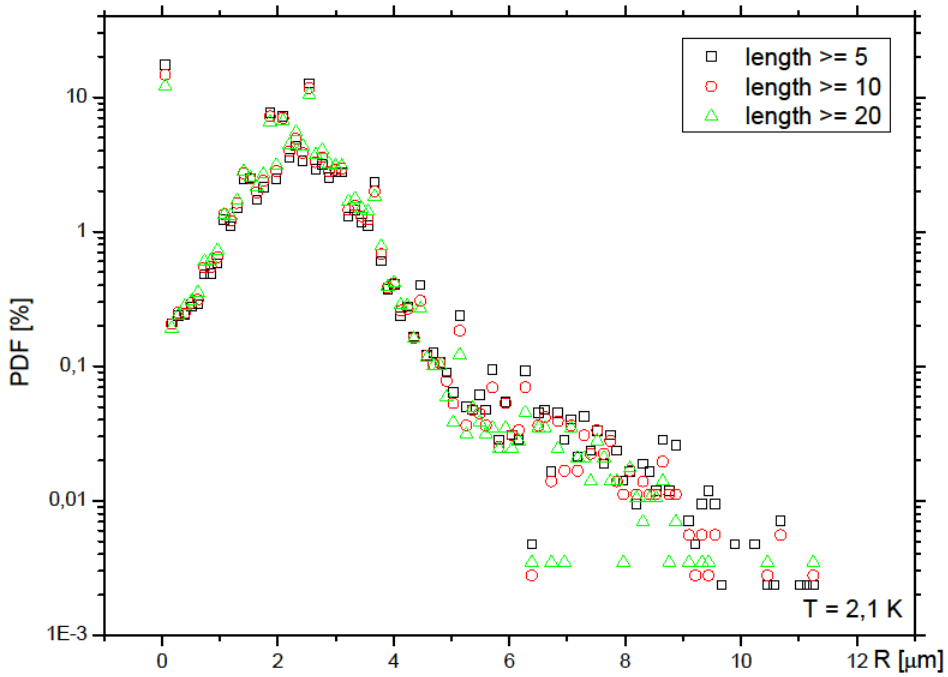

Figure 2.6 *Probability Density Function (PDF) of the radius of the particles. The relevant parameters are: temperature 2,09 K, camera frame rate 100 Hz, laser power 0,3 W (pulse mode with pulse width 6000 µs). Colours correspond to the filter on minimal length of recorded trajectories consisting of number of points as indicated.*

2.9. Illumination

To illuminate the experimental volume a continuous wave solid state laser with tuneable power *Ray Power 5000*, whose maximum power is 5 W, is used. Its wave length is 532 nm (green colour). The power employed in the experiments is usually between 1 and 1,5 W, if the laser operates in continuous mode. Larger power enables us to see smaller particles, but disturbs the results by generating *thermal counterflow* on the heated surface of the particles. This problem is a subject of independent study and detailed quantitative results will be published elsewhere.

To prevent reflections from particles not in the focus plane of the camera, the laser sheet has to be obtained from the laser beam. To do so various lenses are used, see Figure 2.7. The laser sheet employed in most of the experiments reported here has usually a thickness of about 1 mm and its height is about 30 mm.

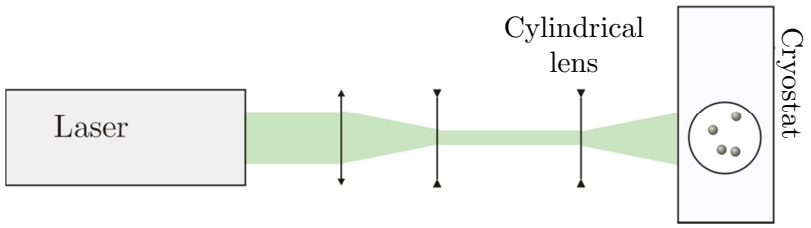

Figure 2.7 *Sketch of the laser sheet formation process. First the laser beam is focused by using a Galileo telescope (converging and diverging lenses), it is then diverged by a cylindrical lens (f = -15 mm) and finally goes into the cryostat. The camera is positioned perpendicularly to the laser sheet, see Figure 1.4.*

The optical part of the apparatus is located on heavy stone tables to reduce vibrations.

2.10. Camera

The used CMOS camera, Phantom v12.1, is very fast: its maximum frame rate at its maximum resolution 1 MP (i. e. 1280 × 800 pixels), is 6273 Hz (or *fps* – frames per second). Its maximum frame rate, 1 MHz, is achieved at the lowest resolution, 128 × 80 pixels. The camera is situated perpendicularly to the illuminated plane and focused on the latter by using an appropriate telemetrical macro lens. The field of view has dimensions of about 13 × 8,2 mm on the focus plane (these dimensions vary slightly, depending on the experiments).

2.11. Software

Data collected during the experiments are processes in different ways. The data on pressure, resistance of thermometers and heater power are recorded by programs written in LabView, which also enables us to switch on and off the heater and the fast needle valve for the injection of particles. These programs were developed in

our laboratory by several people working here during the implementation of the experimental set-up, including myself.

The largest and most important data sets are collected by the camera and recorded by using the commercial software Dynamic Studio, developed by the company Dantec. The software controls the camera and laser, mainly when the latter works in pulse regime. This software also offers a set of various techniques for data analysis, but mostly we do not employ them, as we use for the implementation of the PTV (particle tracking velocimetry) technique other programs. One of them is an opensource add-on to the image analysis software ImageJ. This is called Mosaic and was developed mostly at ETH, Zurich, [17]. This algorithm finds particles on images and connects them to form trajectories, on the basis of a set of chosen parameters, and finally generates a table with the particle positions.

The latter table subsequently serves as the input of a program called *Statistika 1* written by myself, which can smooth trajectories by using the Kolmogorov-Zurbenko algorithm, which is

$\overrightarrow{x_i^s} = \frac{1}{2\mu+1}\sum_{j=i-\mu}^{i+\mu}\overrightarrow{x_j}$, if the point i is at least μ points away from the trajectory final and initial points and

$\overrightarrow{x_i^s} = \overrightarrow{x_i}$, otherwise,

where μ is a chosen parameter. The other chosen parameter is the number of repetitions of this algorithm. The program *Statistika 1* also calculates the velocity in Cartesian coordinates and in local polar coordinates (from the raw or smoothed data). It also computes particle accelerations, lengths of trajectories, percentage of particles moving up and down for each trajectory, mean particle distance from the axis of trajectory, defined as the line passing from the first to the last point of each track, and the statistical errors of all these quantities, obtained from the mean value for each trajectory. For example, the algorithm that obtains the particle velocity from the positions is

$$\begin{aligned}
&\overrightarrow{v_i} = \frac{\overrightarrow{x_{i+1}} - \overrightarrow{x_{i-1}}}{t_{i+1}-t_{i-1}}, \text{ if the point } i \text{ is not the first or the last of the trajectory,}\\
&\overrightarrow{v_i} = \frac{\overrightarrow{x_{i+1}} - \overrightarrow{x_i}}{t_{i+1}-t_i}, \text{ if the point } i \text{ is the first of the trajectory,}\\
&\overrightarrow{v_i} = \frac{\overrightarrow{x_i} - \overrightarrow{x_{i-1}}}{t_i-t_{i-1}}, \text{ if the point } i \text{ is the last of the trajectory,}
\end{aligned} \qquad 2.3$$

where x_i is the position of particle i, at time t_i, and v_i indicates the calculated velocity. It can be said that this algorithm already contains a certain degree of smoothing, as we do not generally know how the particle moves between frames. Besides, this also means that it is not possible to calculate the velocity of a particle, whose trajectory is represented by one point only.

The program produces as output histograms of selected quantities, which can be obtained by considering every point of a chosen data set or by choosing the corresponding averages per trajectory. It can also calculate and plot correlations between any pair of these parameters, see Figure 2.8.

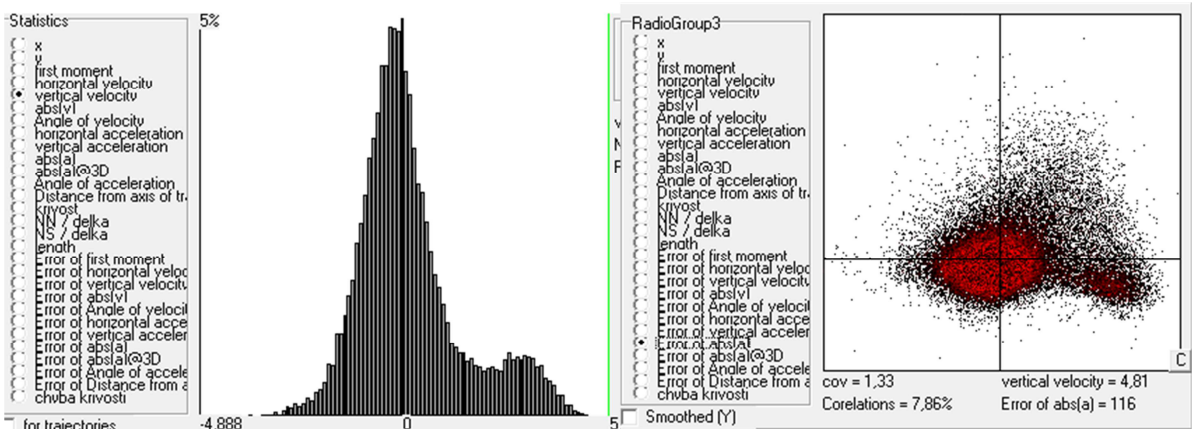

Figure 2.8 *Print screen of typical windows of my program. Left: histogram of the vertical velocity obtained considering every point, for trajectories consisting of at least 5 points, without smoothing. Right: correlation of the latter with the distribution of error of the absolute value of acceleration. The two peaks on the left panel correspond to the fact that there are two types of particles, the firsts going with the normal component and the others with the superfluid component of He II.*

It is also possible to filter the points to be included into the histograms. This can, for example, be done by using as filters the length of trajectories, the maximum optical first moment (to neglect too large particles) and the ratio of points moving up and down for each trajectory (to separate particles carried by the *normal* and *superfluid components*). Besides, it is possible to choose points that are inside or outside user-defined masks, to remove points that are not moving (which generally are bad pixels on the camera sensor or are due to other unphysical effects) and to select points that have a certain quantity lying in a chosen interval.

The program is written in the Delphi language, which is a modern object derivation of the Pascal language and is attached on CD.

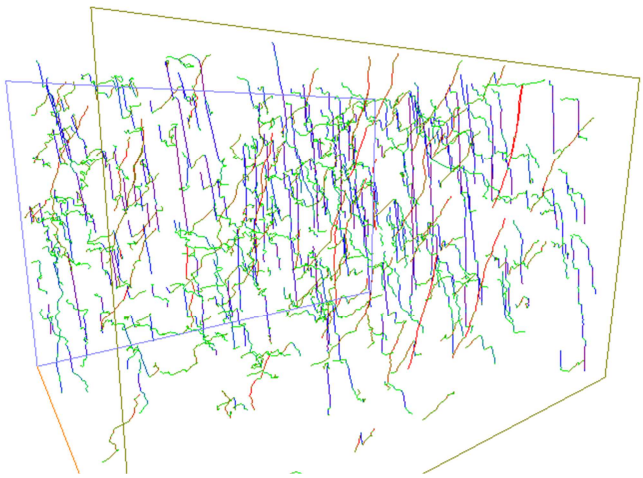

Figure 2.9 *Print screen of the graphical visualization of trajectories, as shown by my software. On the 3rd axis is the time. Colours correspond to vertical velocities. There are only trajectories with at least 50 points.*

3. Results and discussion

3.1. Experimental protocol

The collected videos have typically 1000 frames. Some of them were taken in the absence of heat flux in order to estimate the settling velocities and dimensions of the particles, which have the density about 1,4 times larger than that of liquid helium, if made of solid deuterium. In other movies the heater was switched on in order to study the quantum turbulence generated by the *thermal counterflow*.

The result obtained from movies collected at the same temperature and heat flux were combined, i. e., several movies were generally used to calculate the results shown below for each experimental set of parameters.

3.2. Velocity PDF

The abbreviation PDF stands for the *probability density function* and indicates the probability that a certain quantity has a given value. By using the computer program *Statistika 1* the PDF is obtained as the number of points that have a given property in a chosen subinterval and these points are plotted as a percentage of the number of all included points, i. e., the points that meet the filter chosen conditions.

The PDF of the horizontal instaneous velocity u of solid deuterium particles in thermal *counterflow* is shown in Figure 3.1. (trajectories consisting of at least 5 points were included in the calculations).

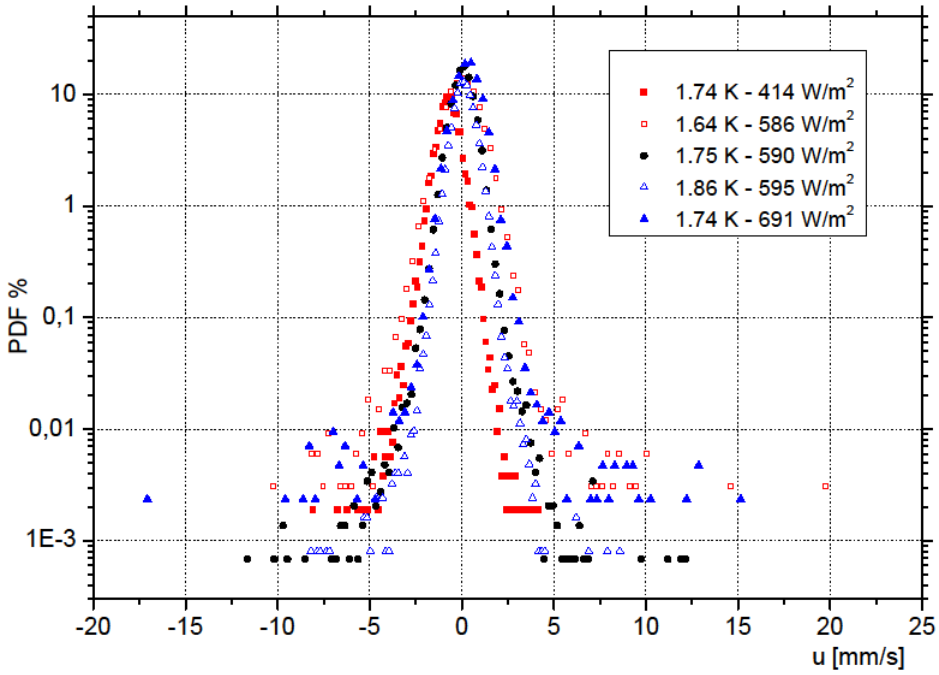

Figure 3.1 *The PDF. of the horizontal velocity of solid deuterium particles in thermal counterflow at various conditions (temperature and heat flux) as indicated*

A more meaningful picture can be obtained by normalizing the data. This is done by subtracting from the experimentally obtained instaneous velocity u the corresponding *average velocity* U and by dividing such a difference by the *standard deviation* u^{sd} of each dataset, as shown in Figure 3.2. The distributions obtained in different experimental conditions can then be compared more easily.

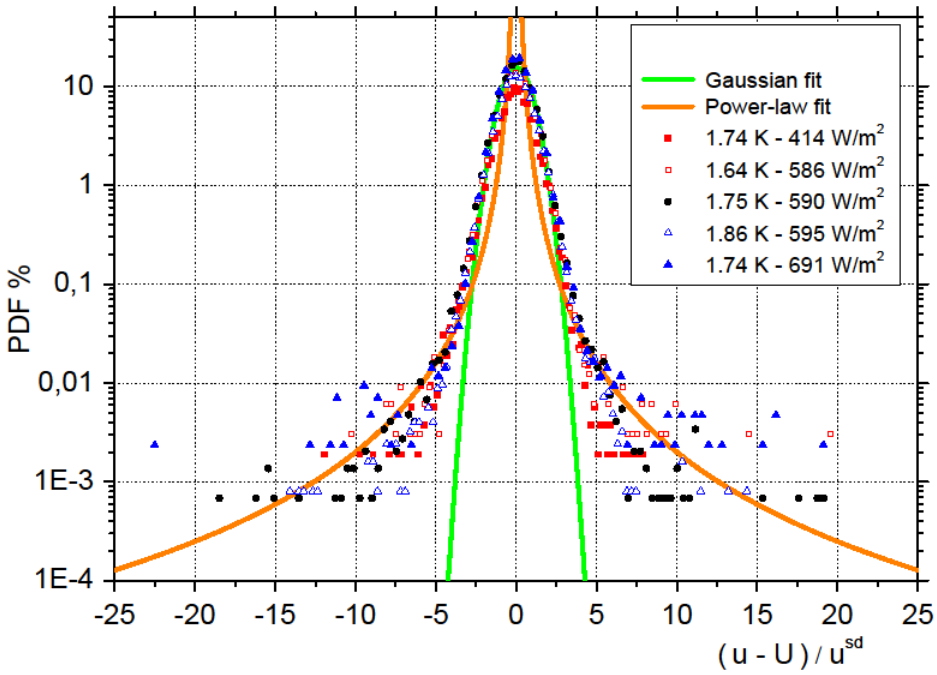

Figure 3.2 *The normalized PDF of the horizontal velocity of solid deuterium particles in thermal counterflow at various conditions (temperature and heat flux) as indicated. Note especially the Gaussian core and non-Gaussian power-law tails.*

The *standard deviation* of the horizontal velocity appears to be related to the calculated *thermal counterflow* velocity v_n, see Figure 3.3. The latter velocity can be obtained from (1.33) as

$$v_n = \frac{q}{\rho s T}, \tag{3.1}$$

where q denotes the heat flux and T indicates the temperature. The density ϱ and specific entropy s, which are tabulated quantities of He II are generally a function of temperature [5]. The relation between v_n and u^{sd} is, however, not entirely understood. It may be linked to the average *distance* between vortex lines l, which can be calculated as

$$l = \frac{1}{\sqrt{L}},$$

where the *vortex line density* L [36] is

$$L = \gamma^2 (v_n - v_s)^2, \tag{3.2}$$

and γ is an experimentally obtained parameter, which, as a first order approximation, can be assumed to increase linearly with increasing temperature; v_n indicates the velocity of the *normal component*, which can be calculated from (3.1), and v_s denotes the velocity of the *superfluid component* and can be obtained from v_n and the conti-

nuity equation (1.28). It could therefore be said that, as v_n increases, the average distance between quantized vortices decreases, leading consequently to an increase in the number of trapping events that may be indirectly observed as the velocity standard deviation increase. The relation between v_n and u^{sd} may also be influenced by the parasitic flows apparent in Figure 3.1.

The *intervortex distances* l calculated by using (3.2) are in this set of parameters (see the legend of Figure 3.1) between 60 and 100 μm, which is comparable with the studied length scale (one pixel in collected images has size equal to 10,2 μm). It can be said that the *intervortex distance* is somewhat analogous to the *Kolmogorov length scale* in a classical turbulence [23]. The argument here is that in classical turbulence the Kolmogorov length scale $\eta = \left(\varepsilon/\nu^3\right)^{1/4}$ based on the dimensional arguments, where $\varepsilon = -dE/dt$ is the energy decay rate. In *superfluid component* we can replace the kinematic viscosity ν by the *circulation quantum* κ. The corresponding length scale, called the *quantum length scale*, is thus of similar size, as by an order of magnitude $\nu \sim \kappa$. The experiments in quantum turbulence thus provide a unique possibility to study the statistical properties of turbulence at length scales smaller than the *Kolmogorov* – or *quantum – length scale*.

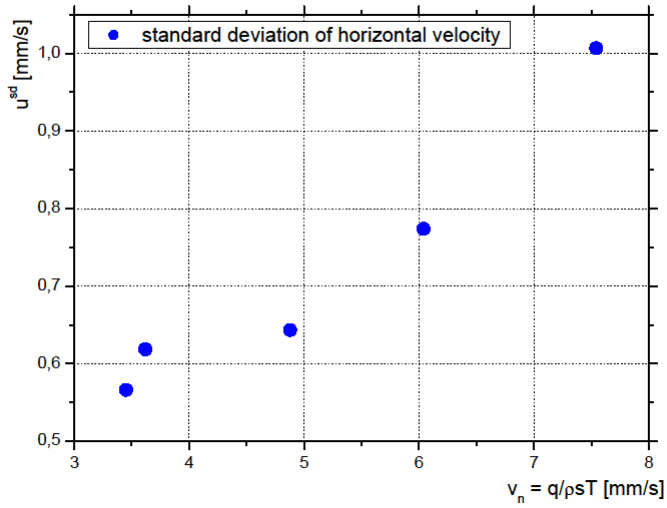

Figure 3.3 *The standard deviation of the distributions shown in* Figure 3.1 *as a function of the corresponding thermal counterflow velocity.*

It seems that the velocities of particles in thermal counterflow have non-classical distributions, which in classical turbulence are usually of a nearly Gaussian shape, see Figure 3.2. The velocity distributions display indeed a non-Gaussian form with power-law tails, which are, according to [19], due to the superfluid velocity behaviour around vortex filaments. This non-classical shape of the velocity distribution can be seen as a fundamental property of He II quantum turbulence, which can be described as resulting from the dynamical behaviour of a tangle of quantized vortices – the line singularities in the macroscopic wave function of the *superfluid component* of He II, as mentioned above.

If we consider one straight quantized vortex running along the axis of cylindrical volume, the corresponding velocity field can be written, relatively to the quantized vortex core and according to (1.31), as

$$\overrightarrow{v_s} = \frac{h}{2\pi m}\left(\frac{y}{x^2+y^2}, -\frac{x}{x^2+y^2}, 0\right),$$

where h/m is the *quantum of circulation* κ. The velocity distribution per unit volume can be defined as

$$\mathcal{D}(v) = \int \delta(v - |\vec{v}(\vec{x})|)d\vec{x}.$$

The latter, by assuming $|\vec{v}(\vec{x})| = \frac{\hbar}{m}\frac{1}{r} =: v^*$, where $r = |\vec{x}|$, can finally be written as

$$\mathcal{D}(v) = \int \delta(v - v^*)\frac{-\hbar^2}{m^2}\frac{1}{v^*}\frac{1}{v^{*2}}dv^* = \frac{\hbar^2}{m^2}\frac{1}{v^3}. \qquad 3.3$$

This result, calculated in very special conditions, agrees with the shape of the tails of the *probability density function* of the horizontal velocity shown in Figure 3.2. The tails correspond to the largest velocities of the particles, those orbiting closer to the vortex lines. The core of the distribution of the particle velocities is more similar to the *Gaussian distribution* because the particles are here affected by more than one quantized vortex line, resulting in averaging and smoothing the large velocity departures. The quasi-classical behaviour dominates then at length scales larger than the intervortex distance.

The distribution of the vertical velocity has usually two peaks, see, for example, Figure 3.4. These peaks are due to the fact that some particles follow the *normal component* of He II, while others are trapped into quantized vortices.

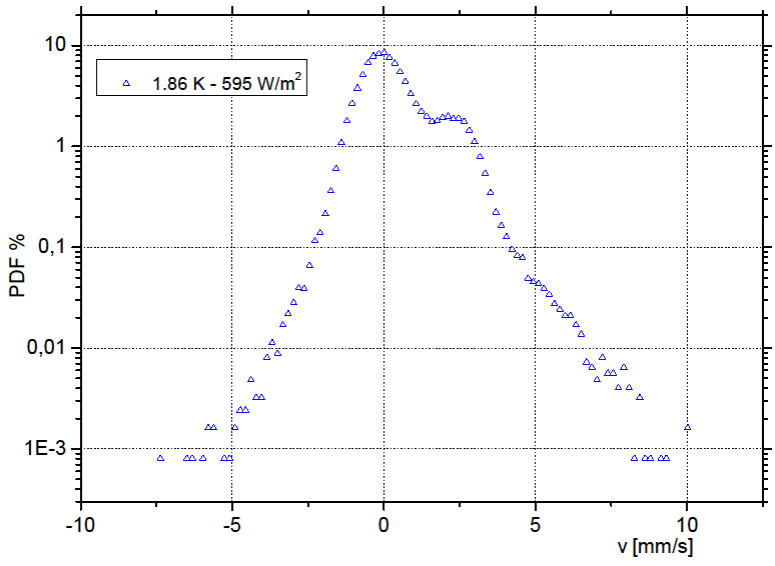

Figure 3.4 *The distribution of the vertical velocity at temperature 1,86 K and heat flux 595 W/m². The negative values of velocity correspond to the up direction, i. e., to the normal fluid direction.*

The behaviour shown in Figure 3.4 has not a classical analogue; in other words the two peaks are not due to a convective flow, but are the consequence of the

quantum nature of He II. In the studied videos particles moving up can be seen together with homogenously located particles moving down.

The behaviour of *standard deviation* of vertical velocity is qualitatively similar to the one of horizontal velocity shown in Figure 3.3, but it is also influenced by the *distance* of the peaks in Figure 3.4 and the interpretation of its behaviour is more complex and poorly understood.

3.3. Acceleration PDF

The accelerations are calculated numerically in a way similar to the velocities; see equation (2.3) and replace a, i. e. acceleration, with v and v with x. The *probability density function* of the particle acceleration in the vertical direction is displayed in Figure 3.5 and Figure 3.6 (results obtained from the same datasets used above are plotted).

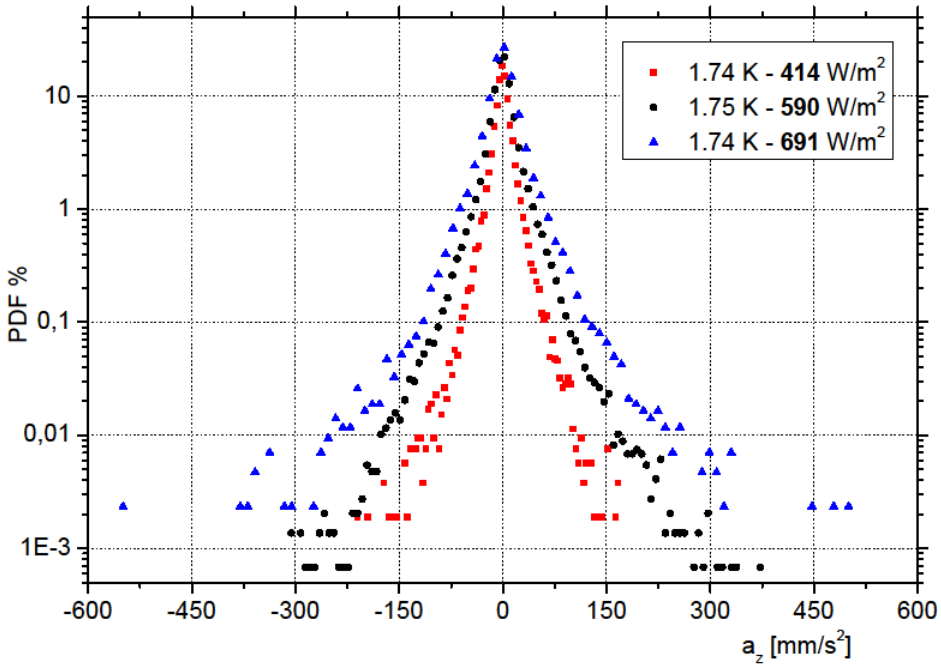

Figure 3.5 *The PDF of the vertical acceleration at temperature equal to approximately 1,75 K and different heat fluxes (trajectories with at least 5 points) as indicated.*

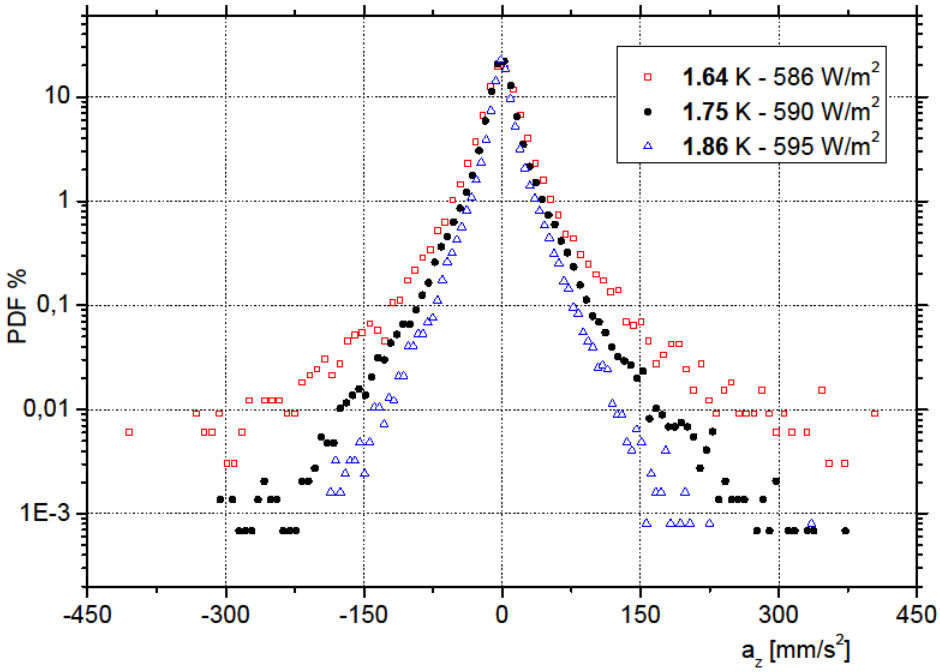

Figure 3.6 *The PDF of the vertical acceleration at heat flux equal approximately 590 W/m² and different temperatures as indicated.*

It is possible to see that the tails of the distributions become wider as the *temperature* decreases and *heat flux* increases. The same was observed for the instantaneous horizontal acceleration a_x. We can assume that the accelerations in horizontal planes, i. e. a_x and a_y, are equal, due to the symmetry of the vertical *counterflow*. An average acceleration amplitude A can then be defined as the ensemble average of the instantaneous accelerations, i. e.

$$A = \langle \sqrt{2 \cdot a_x^2 + a_z^2} \rangle.$$

A also increases as temperature decreases and heat flux increases, see Figure 3.7

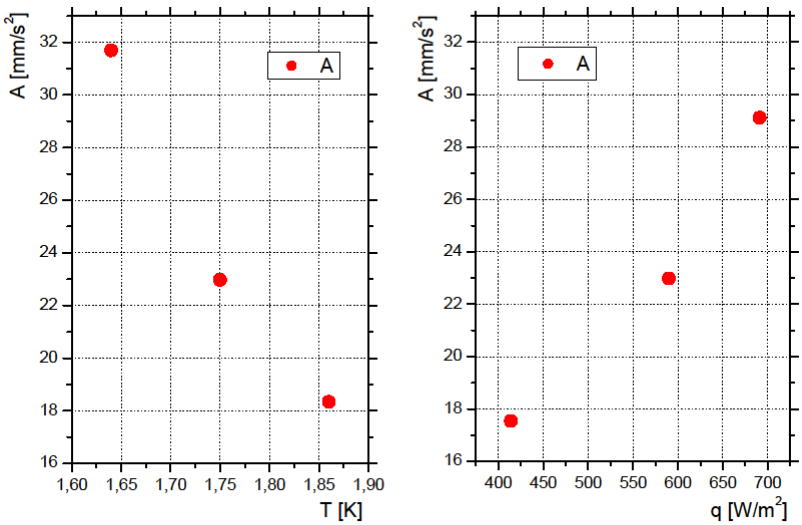

Figure 3.7 *Left panel: A as a function of temperature, at heat flux approximately equal to 590 W/m²; right: A as a function of heat flux, at temperature around 1,75 K.*

The just mentioned result, shown in Figure 3.7, can also be displayed as the dependence of A on the calculated *thermal counterflow* velocity defined by (3.1), see Figure 3.8.

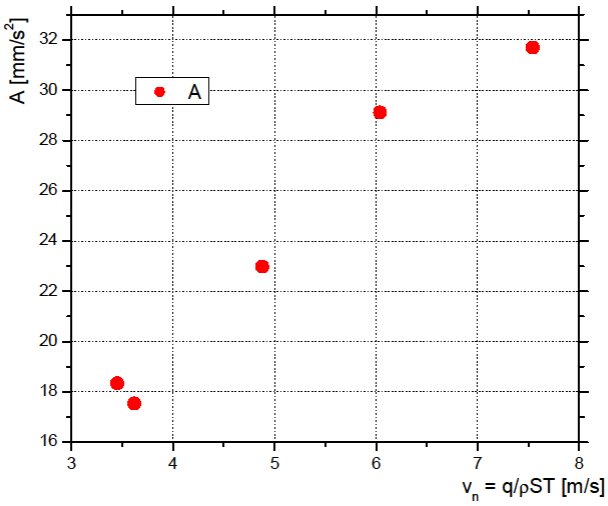

Figure 3.8 *The average of the acceleration amplitude as a function of* v_n, (3.1).

A more interesting picture of the vertical acceleration distributions can be obtained by dividing the accelerations by the corresponding *standard deviation*, that is, by normalizing the data. The distributions obtained in different experimental conditions can then be compared more easily.

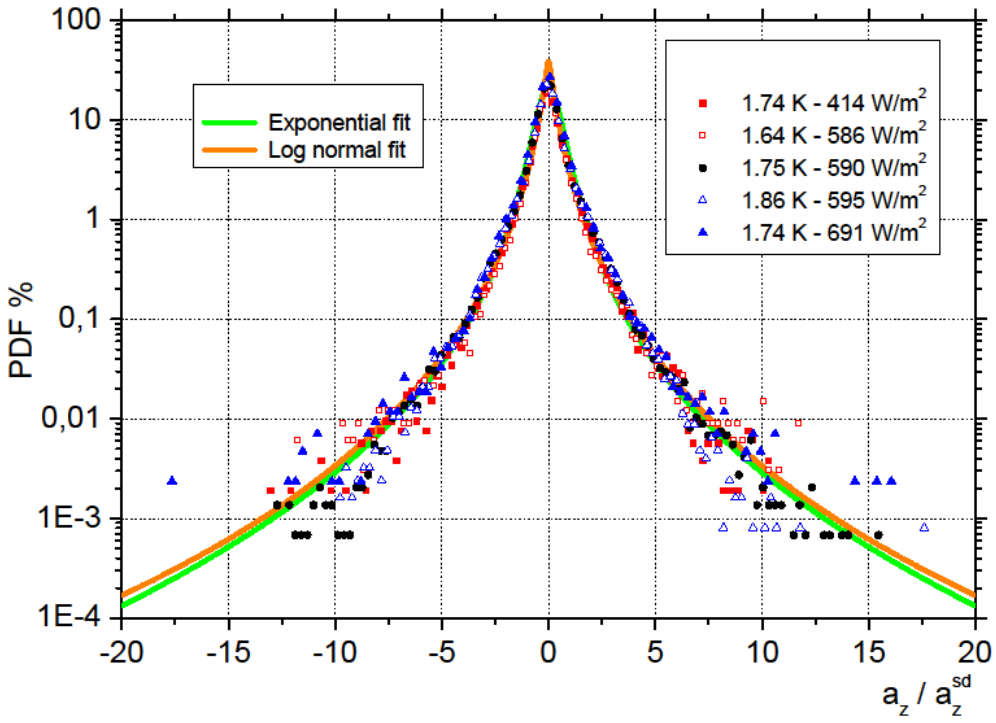

Figure 3.9 *The normalized PDF of the particles vertical acceleration at various conditions (i. e. temperature and heat flux as indicated);* a_z^{sd} *is the standard deviation of* a_z.

The normalized distribution of the particle vertical accelerations, shown in Figure 3.9, can be approximated by the *exponential* curve used to fit the data obtained from classical turbulent flows in water, [20], i. e.

$$\mathcal{D}(a) = C \cdot \exp\left[\frac{-a^2}{\left(1+\left|\frac{\alpha\beta}{\sigma}\right|^{\gamma}\right)\cdot\sigma^2}\right], \tag{3.4}$$

where $\mathcal{D}(a)$ is the probability density function of the normalized acceleration, $\beta = 0{,}513$, $\sigma = 0{,}563$, $\gamma = 1{,}600$ [20] and $C = 21{,}99$, which is 30 times larger than that used in [20] as the PDF is normalized differently. It seems then that the observed particle accelerations in He II follow a classical-like behaviour, at the probed length-scales.

It is possible to use another fit, based on the *log-normal* distribution, shown in Figure 3.9, and also obtained for classical turbulent flows [21]. It is defined as

$$\mathcal{D}(a) = N \cdot \frac{\exp\left[\frac{3s^2}{2}\right]}{4\sqrt{3}} \cdot \left(1 - \operatorname{erf}\left[\frac{ln\left|\frac{a}{\sqrt{3}}\right| + 2s^2}{\sqrt{2}s}\right]\right), \tag{3.5}$$

where $s = 1$ [21] and $N = 30$, which is 30 times larger than the value used in [21], as the PDF is normalized differently. Besides, the *flatness* of the distribution is estimated to be around 20 but it was not possible to calculate it accurately, because the obtained data sets are smaller than those used in classical turbulence studies.

The simple model, used above for the velocities, equation (3.3), leads, in the case of accelerations, by considering that the acceleration of a superfluid particle orbiting a vortex filament is

$$a(r) = \frac{v^2}{r} = \frac{1}{(2\pi)^2}\frac{\kappa^2}{r^3},$$

to the distribution of the form

$$\mathcal{D}(a) = \int \delta\big(a - a(r)\big) r dr = \frac{1}{3}\left(\frac{\hbar}{m}\right)^{4/3} \frac{1}{a^{5/3}}, \tag{3.6}$$

which, at large enough accelerations, appears to be quite similar to the classical behaviour, see (3.4) and (3.5). It is however not possible to differentiate the shapes clearly, in the range of investigated parameters, as the used number of points in the statistics it is not sufficient to do so.

Another parameter, employed to describe the obtained results can be defined as the ratio between the viscous drag force, per unit of mass, due to the *normal component* of He II, acting on the particle, and the pressure gradient force, per unit of mass, due to the *superfluid component* of He II, attracting the particle to a superfluid vortex filament, i. e.

$$\Lambda = \frac{\frac{9\mu_n}{2\rho_0 R_p^2}\left(V_n - v_p\right)}{\frac{3\rho_s}{2\rho_0}\frac{\kappa^2}{8\pi^2}\nabla\left(\frac{1}{r^2}\right)}, \tag{3.7}$$

where V_n denotes the mean velocity of the *normal component* of He II, v_p is the velocity of the particle, μ_n indicates the dynamic viscosity of the *normal component* of

He II and R_p is the radius of the particle; κ denotes the quantum of circulation, see (1.30), and the *gradient* of $1/r^2$ is derived from the *Bernoulli equation* (1.36) and from the fact that the velocity around a quantized vortex core depends on the distance r from it as $1/r$, see (1.31).

Assuming, that the radius R_p of the particle is constant, the ratio Λ is proportional to another parameter

$$\zeta = \frac{\mu_n(V_n - v_p)}{\rho_s}, \tag{3.8}$$

of dimension [m^3/s^2]. Note that the average velocity of the *normal component* of He II can be approximated by the calculated *thermal counterflow* velocity v_n (3.1) while the particle velocity v_p can be replaced by the experimentally obtained mean vertical velocity. Other parameters, i. e., the dynamic viscosity μ_n and the density of the *superfluid component* ϱ_s are functions of temperature and are tabulated.

As T decreases or q increases, ζ increases similarly to the acceleration magnitude A. Note that the dependence of A on ζ is similar to the dependence on v_n, shown in Figure 3.8, as v_n is linearly dependent on ζ, see (3.8).

The behaviour of A and ζ is shown in Table 3.1 and Table 3.2, as a function of applied heat flux and temperature, respectively. The qualitative dependence can be seen as the result of the fact that particles are less likely trapped into vortices, as temperature increases and heat flux decreases. This means that when a particle is trapped, it stays so for shorter time and this leads consequently to more frequent changes of particle velocity, i. e. to larger particle acceleration.

Table 3.1 *Qualitative dependence of the average acceleration magnitude A and parameter ζ on applied heat flux q, at temperature around 1,75 K.*

	A increases by	ζ increases by
q increases from 414 to 590 W/m^2	31 %	23 %
q increases from 590 to 691 W/m^2	27 %	21 %
q increases from 414 to 691 W/m^2	66 %	50 %

Table 3.2 *Qualitative dependence of the average acceleration magnitude A and parameter ζ on the temperature, at applied heat flux around 588 W/m^2.*

	A increases by	ζ increases by
T decreases from 1.86 to 1.75 K	25 %	25 %
T decreases from 1.75 to 1.64 K	38 %	22 %
T decreases from 1.86 to 1.64 K	73 %	52 %

In other words, the pressure gradient force would affect the trajectories of the particles and consequently the corresponding velocities and accelerations, without leading to long-lasting particle trapping events [22]. The fact that the distribution of particle radii is not sharp, see, for example, Figure 2.6, can also affect the results. Moreover, the model of particle motion, used for the derivation of (3.7), is valid if the particle *Reynolds numbers*, defined below by equation (3.9), is lower than 1 and in the present case the particle *Reynolds number* is around 1. For a particle moving in He II the *Reynolds number* can be estimated as

$$Re_p = \frac{2\rho_n}{\mu_n} R_p \cdot (V_n - v_p), \tag{3.9}$$

which is obtained by only considering the *normal component* of He II.

3.4. Future work

Future plans include the study flows past bluff bodies. As a first step, the *thermal counterflow* past a cylinder is being investigated and corresponding preliminary results are here reported. The experiments with a cylinder were performed by using the setup shown in Figure 2.4, which was designed and built also thanks to my contribution. The black painted cylinder was made from brass and has diameter of 3 mm and length of 27 mm, spanning the cell width; it is fixed externally to the glass wall of the cell by a nut. The laser sheet is perpendicular to the axis of the cylinder and the camera is oriented accordingly. The establishing of the data-analysis-protocol is in progress.

One of the aims of the experiment is to verify that, as reported in the literature [12], macroscopic vortices are shed also in the *superfluid* flow direction and not just in the *normal fluid* flow direction, as in classical flows past bluff bodies.

Thermal counterflow due to heated cylinder

During the first experiments *thermal counterflow* originating from the cylinder surface was observed, as the cylinder was heated by the laser light (the cylinder surface was painted in black to avoid reflections).

The used laser power was about 1,4 W. If we assume, for the sake of simplicity, that the intensity profile of the obtained laser beam is a *step function*, instead of being *Gaussian*, the power reaching the cylinder can be estimated to be about 9 mW. This means that the thermal irradiation from the illuminated surface ($\pi/2$ times larger than the cylinder diameter) is around 600 W/m^2 in the vicinity of the cylinder surface (note that, in cylindrical coordinates, the heat flux decreases as $1/r$, where r is the distance from the cylinder axis, and that the thermal conductance of brass and black paint are negligible, if compared with the thermal conductance of He II due to the superfluid convection). We also assume that the surface absorbs all the incoming light, even though this is not entirely true due to the presence of deuterium particles in the proximity of the cylinder and due to non-zero reflexivity of the cylinder.

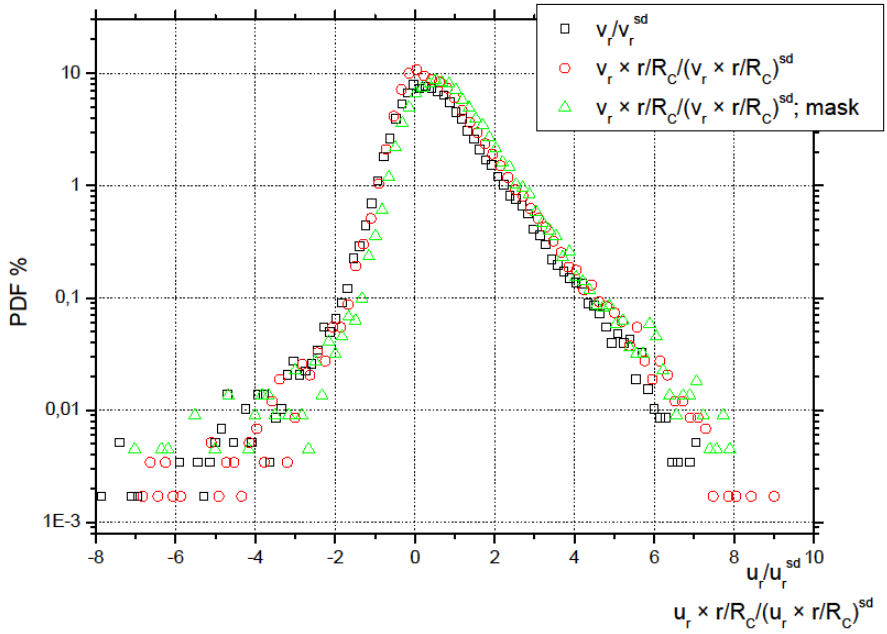

Figure 3.10 *The PDF of the radial component of the normalized velocity near the cylinder is shown as open black squares; open red circles denote the PDF of the radial component of the velocity normalized by taking into account the distance r from the cylinder of radius R_p; open green triangles indicate the latter normalized velocity in a selected area near the cylinder. Data are taken at temperature 1,9 K and laser power 1,4 W (heater switched off).*

The *thermal counterflow* generated by the heated cylinder is studied in cylindrical coordinates and the corresponding velocities are obtained as

$$v_i^r = v_i^x \cdot \frac{r_i^x}{r_i} + v_i^y \cdot \frac{r_i^y}{r_i},$$

where r^x and r^y are the components of the distance r_i from the axis of the cylinder, respectively, in the Cartesian frame of reference. The distributions of the radial component of the particle velocity are shown in Figure 3.10.

As it was mentioned above, the local heat flux decreases as the distance from the cylinder increases. We can therefore normalize the radial velocity w as

$$w_i^r = v_i^r \cdot \frac{r_i}{R_C},$$

where R_C is the radius of the cylinder, i. e. 1,5 mm. The average velocity of the particles moving away from the cylinder is equal to 1,2 mm/s in the case shown in the Figure 3.10. By using equation (1.33) we can estimate the heat flux at the cylinder surface to be about 240 W/m^2, which is $2/5$ of the value obtained above. Data from a selected area in the proximity of the cylinder are also plotted in Figure 3.10 (green triangles) to neglect the effect of inhomogenous heating of the cylinder surface. The corresponding result is however similar, being around 250 W/m^2. Note also that the outcome is consistent with the experimental observation, obtained in several counterflow experiments, that the measured particle velocity is generally smaller than the calculated one, see, for example, [14].

It can be said that the particle motion is indeed affected by the heated cylinder surfaceand for our future investigations we plan to use a transparent cylinder in order to reduce this effect.

Classical vortices due to the residual flow

A number of large vortical structures were observed in the flow around the cylinder. These structures do not seem to be due to the applied heater power but might be the result of the residual flow in the bath generated during the injection of the particles.

In this case we can consider that the two *components* of He II move more or less together. It is then possible to use the algorithms developed for classical fluids based on equation (1.35) and implemented in the software Dynamic Studio. A corresponding outcome is shown in Figure 3.11.

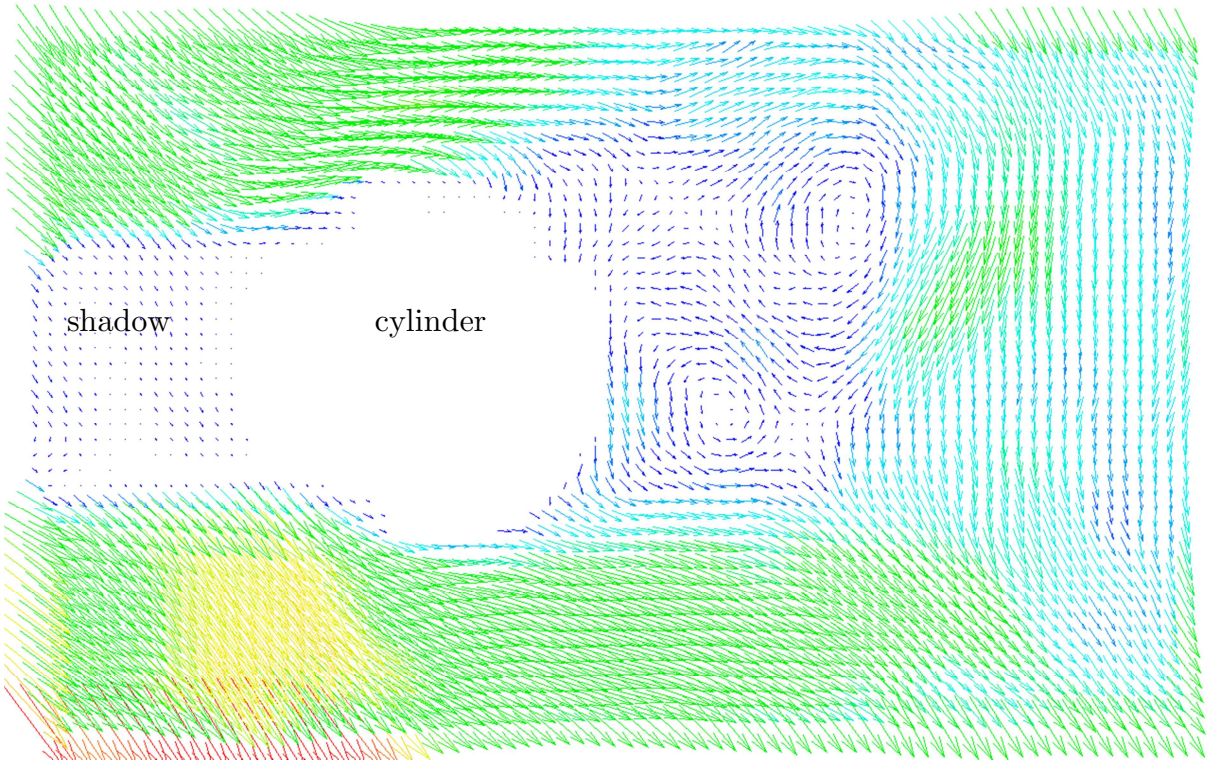

Figure 3.11 *The vector map of the particle velocity around the cylinder. The length and colour of the vectors correspond to the absolute value of velocity; the maximum velocity, red colour, is 4 mm/s. The temperature is 2,16 K, there is not additional heat flux, the laser power is 1,1 W. Data in the shadow behind the cylinder are not relevant.*

The study of the classical-like vortices is not the main topic of our work. Nevertheless we see that a macroscopic vortex can exist in He II, at least in the *normal component*.

The analysis of the current cylinder data is in progress, and a new transparent cylinder, made of plexiglass, will be used for the next experiments.

4. Conclusion

Quantum turbulence in *superfluid helium*, generated by *thermal counterflow*, was studied by using the PTV (particle tracking velocimetry) technique. Micrometre-sized particles were generated and injected into the He II bath inside a low-loss cryostat with optical ports to enable flow visualisation measurements. The particles were illuminated by a solid state laser and their motion was observed by a digital camera. The collected images were processes by purpose-made computer programs (one of these was developed by me). Once particles were found in the images their velocities and accelerations were calculated numerically.

The distribution of longitudinal (vertical) velocities of particles, moving in *thermal counterflow*, reflects *two fluid behaviour* of He II, see Figure 3.4. Particles moving away from the heat source, carried by the *normal component* of He II, owing to the viscous drag force, and particles moving in opposite direction as being trapped into *quantized vortices*, were observed. These two flows – or types of behaviour of particles – were located homogenously in the studied volume. The result proves that *thermal counterflow* has no analogue in classical fluids and represents a unique type of convective flow possible only in quantum liquids.

The shape of the normalized probability density function of the velocity v of the particles serves as a clear indication of the quantum nature of *thermal counterflow*. The distribution core, which corresponds to small values of velocity, has a shape similar to that of the *Gaussian distribution*, which can be regarded as the form of the velocity distribution in classical turbulent flows. At larger values of velocity the behaviour is completely different and the distribution tails have a power-law form, proportional to $1/v^3$. The latter can be understood by considering the superfluid velocity around a quantized vortex, inversely proportional to the distance from the vortex core.

The normalized distribution of the particle acceleration appears to follow, in the range of investigated parameters, an unexpected classical-like behaviour, while the shapes of velocity distribution are clearly different. This problem should be addressed using larger data sets, obtained at larger frame rates.

The velocity and temperature dependence of the average amplitude of the acceleration can be qualitatively explained by exploiting the two fluid model of *thermal counterflow*: by looking at the ratio between the viscous drag force, acting on the particles in the velocity field of the *normal component* of He II, and the *Bernoulli gradient* force, attracting the particles to quantized vortices in the velocity field of the *superfluid component* of He II. This, together with the power-law form of the velocity distribution, can be regarded as a quantum signature of *thermal counterflow*, clearly distinguishing classical and quantum turbulence flows.

List of references

[1] Ladislav Skrbek a kol., Fyzika nízkých teplot, MatfyzPress, Praha 2011

[2] Echelle internationale de temperature de 1990, BIPM, Paris 1989

[3] Jiří Englich, Zpracování výsledků fyzikálních měření, MatfyzPress, Praha 2002

[4] Miroslav Brdička, Ladislav Samek, Bruno Sopko, Mechanika kontinua, Academia, Praha 2000

[5] Thomas M. Flynn, Cryogenic Engineering, CRC Press, Boca Raton 2005

[6] Ch. Kittel: Úvod do fyziky pevných látek, Academia, Praha 1985

[7] R. S. Šafrata, Z. Janů, M. Rotter, M. Koláč, B. Sedlák, L. Skrbek a M. Trhlík: Fyzika nízkých teplot, MatfyzPress, Praha 1998

[8] D. R. Tilley, J. Tilley, Superfluidity and Superconductivity, Institute of Physics Publishing, Bristol and Philadelphia 1990

[9] T. J. Qiunn: Temperature, Academic Press, London 1990

[10] Daniel Duda, Nekovové odporové termometry nízkých teplot, Bakalářská práce MFF UK, Praha 2011

[11] F. W. Vinen, J. J. Niemela, Quantum turbulence, Journal of Low Temperature Physics, 128, Nos. 5/6, September 2002

[12] Tao Zhang, Steven W. Van Sciver, Large-scale turbulent flow around a cylinder in counterflow superfluid ^{4}He, Nature Physics 1, 36, October 2005

[13] H. E. Hall, W. F. Vinen, The rotation of liquid helium II, Proc. Roy. Soc. A 238 204, 215, 1956

[14] M. La Mantia, T. V. Chagovets, M. Rotter and L. Skrbek, Testing the performance of a cryogenic visualization system on thermal counterflow by using hydrogen and deuterium solid tracers, Rev. Sci. Instrum. 83, 055109, 2012

[15] G. P. Bewley, K. R. Sreenivasan, and D. P. Lathrop, Exp. Fluids 44, 887, 2008

[16] Л. Д. Ландау, Е. М. Лифшиц, Гидродинамика, Наука, Москва 1986

[17] I. F. Sbalzarini, P. Koumoutsakos, Feature point tracking and trajectory analysis for video imaging in cell biology, J. Struct. Biol. 151, 182-195, 2005

[18] M. La Mantia, D. Duda, M. Rotter, L. Skrbek, Lagrange accelerations of particles in superfluid turbulence, J. Fluid Mech., vol. 717, R9, 2013

[19] A. C. White, C. F. Barenghi, N. P. Proukakis, A. J. Youd, D. H. Wacks, Nonclassical velocity statistics in a turbulent atomic Bose-Einstein condensate, Phys. Rev. Lett., 104, 075301, 2010

[20] N. Mordant, A. M. Crawford, E. Bodenschatz, Experimental Lagrangian accelerationprobability density function measurement, Physica D 193, 245-251, 2004a

[21] N. Mordant, A. M. Crawford, E. Bodenschatz, Three-dimensional structure of the Lagrangian acceleration in turbulent flows, Phys. Rev. Lett. 93, 214501, 2004b

[22] Y. A. Sergeev, S. Wangs, E. Meneguz, C. F. Barenghi, Influence of normal fluid disturbances on interactions of solid particles with quantized vortices, J. Loe Temp. Phys., 146, 417-434, 2007

[23] Václav Uruba, Turbulence, Nakladatelství ČVUT, Praha 2009

[24] Y. A. Sergeev, C. F. Barenghi, D. Kivotides, Motion of micron-size particles in turbulent helium II, Phys. Rev. B 74, 184506, 2006

[25] D. R. Poole, C. F. Barenghi, Y. A. Sergeev, W. F. Vinen, Motion of tracer particles in He II, Phys. Rev. B 71, 064514, 2005

[26] G. P. Bewley, D. P. Lathrop, K. R. Sreenivasan, Visualization of quantized vortices, Nature, 588, 2006

[27] Veronika Pilcová, Visualization of selected flows of water and cryogenic helium using tracer particles, Diplomová práce MFF UK, Praha 2011

[28] O. C. Idowu, A. Willis, C. F. Barenghi, D. C. Samuels, Local normal-fluid helium II flow due to mutual friction interaction with the superfluid, Phys. Rev. B 62, 3409, 2000

[29] G. P. Bewley, K. R. Sreenivasan, D. P. Lathrop, Particles for tracing turbulent liquid helium, Exp Fluids 44, 887, 2008

[30] L. Skrbek, Turbulence in cryogenic helium, Physica C 404, 354, 2004

[31] E. J. Yarmchuk, R. E. Packard, Photographic studies of quantized vortex lines, J Low Temp. Phys. 46, 479 – 515, 1982

[32] Frank Pobell, Matter and Methods at Low Temperatures, Springer, Berlin Heidelberg 2007

[33] Josef Jelínek, Zdeněk Málek, Kryogenní technika, Státní nakladatelství technické literatury, Praha 1982

[34] Jaroslav Vepřek, Elektrická měření nízkých teplot, Státní nakladatelství technické literatury, 1977

[35] Stephen C. Bates, Compilation of the engineering properties of solid hydrogen, Glastonbury 2002

[36] Sergey K. Nemirovskii, Fluctuations of the vortex line density in turbulent flows of quantum liquids, Phys. Rev. B, 86, 224505, 20012